Sapienza University of Rome

School of Biology and Molecular Medicine

PhD Thesis

"Characterization of molecular bases of Myhre syndrome"

PhD course

Human Biology and Medical Genetics

Medical Genetics *curriculum*

XXVIII cycle

Coordinator: Prof. Antonio Pizzuti

Tutor: Dr. Viviana Caputo

Candidate: Dr. Alice Traversa

Index

Abstract

Myhre syndrome (MYHRS, MIM 139210) is a rare developmental disorder first described in 1981, for which about 50 cases are currently reported. Clinical features of MHYRS include typical facial gestalt (short palpebral fissures and philtrum, mid-face hypoplasia, prognathism, narrow mouth), thickened skin, joint limitation, muscular pseudohypertrophy, mild-to-moderate intellectual deficiency and hearing loss.

Our group (Caputo *et al.*, 2012) and others (Le Goff *et al.*, 2011a) identified *SMAD4* (MIM 600993) as the gene mutated in MYHRS using Whole Exome Sequencing approach. Three different *de novo* missense changes involving Isoleucine 500 (p.Ile500Thr, p.Ile500Val and p.Ile500Met) within the evolutionary conserved MAD homology 2 domain of SMAD4 were detected in 19 patients.

SMAD4 plays a pivotal role in signal transduction of the transforming growth factor beta (TGFβ) superfamily cytokines, which exerts an important role from early embryogenesis to adulthood by mediating transcriptional activation of target genes involved in different cellular processes (such as cell division, differentiation, migration, and programmed cell death). *SMAD4* has been established as a tumor suppressor gene, since loss-of-function mutations are known to cause two familiar cancer-prone diseases (juvenile polyposis syndrome (JPS, MIM 174900) and Juvenile polyposis/hereditary hemorrhagic telangiectasia (JPHT, MIM 175050), Gallione *et al.*, 2004; Gallione *et al.*, 2010), and occur in different types of carcinomas (pancreas, gastrointestinal tract and skin).

The main purpose of this thesis was the investigation of the molecular bases of Myhre syndrome through functional and *in silico* approaches. Molecular studies and assays on cell cultures were performed in order to characterize MYHRS causative variants.

Firstly, different cellular and biochemical assays were performed, in order to assess MYHRS Ile500 mutations functional impact on SMAD4 protein expression, localization, and on cell proliferation. Western blot analysis of MYHRS fibroblasts and HeLa SMAD4-mutated transfected cells, showed an increased endogenous and ectopic expression of the protein, respectively. Immunofluorescence analysis by confocal laser scanning microscopy of MYHRS fibroblasts disclosed an extra-nuclear accumulation of MYHRS-mutated SMAD4 in patient fibroblasts after 2.5 and 5 hours of TGFβ stimulation. Growth curve of MYHRS-mutated fibroblasts, as well as BrdU incorporation assay on MYHRS fibroblasts and 3T3 transfected

cells, demonstrated a reduction in the proliferation levels of both patient and SMAD4-mutated overexpressing cells.

Moreover, we collected a cohort of cases with clinical features fitting MYHRS. Molecular screening of *SMAD4* coding sequence in these patients identified a novel missense change affecting Arginine 496 (p.Arg496Cys) in three cases. *In silico* structural analysis, performed in collaboration with Tor Vergata University, suggested that conformational changes promoted by replacement of Arg496 impact the stability of the SMAD heterotrimer and/or proper SMAD4 ubiquitination (Caputo *et al.*, 2014). Since the triplet coding for the Arginine at position 496 encompassed a CpG dinucleotide, we preliminarily investigated the methylation status of the cytosine at nucleotide c.1486, through digestion assays of genomic DNA from leukocytes of control subjects with Hpy99I methylation sensitive restriction enzyme which confirmed that c.1486 C>T mutation localized in a methylated CpG dinucleotide.

Finally, the investigation of the parental germline origin of MYHRS mutations was performed. Cloning of genomic fragments encompassing *SMAD4* causative mutation and intronic polymorphic site for 11 informative MYHRS cases and segregation analysis demonstrated the paternal germline origin of Myhre pathogenic variants in all these patients, in line with the well-known gender bias in the origin of point mutations.

In conclusion, our functional data confirm increased expression of Ile500-mutated SMAD4 in MYHRS affected cells and point out a loss of function effect of MYHRS mutations on fibroblasts proliferation, a mechanism activated by TGFβ signaling. Furthermore, the identification of a new mutation causing this syndrome (c.1486 C>T; p.Arg496Cys), which encompass an amino acid close to Ile500 residue, suggests the impairment of ubiquitination and/or transcription complex stability as the probable outcome of this variant, highlighting the need of further investigations on possible different effect of MYHRS mutations on TGFβ signaling and gene transcription. Finally, the exclusive paternal origin of MYHRS variants in our 11 informative patients expand the number of point mutations causing dominant disorders which display a paternal bias in origin, and lead us to speculate on possibly other mechanisms which could produce a positive selection on MYHRS mutations in male testes.

1. Introduction

1.1 Myhre syndrome: historical overview

Myhre syndrome (MYHRS, MIM 139210) is a rare developmental disorder, with less than 50 cases currently reported. This syndrome was first described in 1981 for two unrelated male patients (Myhre *et al.*, 1981) who showed similar dysmorphic features not attributable to a previously recognized syndrome. Both cases exhibited mental retardation, prenatal and postnatal growth deficiency, unusual facies (maxillar hypoplasia, prognathism, short palpebral fessures and philtrum), skeletal anomalies (thickened calvarium, prominent broad mandible, hypoplastic iliac wings, broad ribs, shortened tubular bones and large, flattened, non-beacked vertebrae with large pedicles), generalized muscular hypertrophy and joint limitations. Additional findings reported were cardiac anomalies, cryptorchidism, and severe mixed hearing loss. Other nine male patients with MYHRS phenotype were described later on (Burglen *et al.*, 2003; Garcia-Cruz *et al.*, 1993; Soljak *et al.*, 1983; Titomanlio *et al.*, 2001; Whiteford *et al.*, 2001), among them some showing also behavior problems like autism (Titomanlio *et al.*, 2001) and hyperactivity (Burglen *et al.* 2003). In 2003 Davalos *et al.* reported on the first female case, suggesting that MYHRS could be caused by a *de novo* dominant mutation, since the advanced paternal age at the time of conception. After that, the discovery of other 6 female patients (Bachmann-Gagescu *et al.*, 2011; Becerra-Solano *et al.*, 2008; Lopez-Cardona *et al.*, 2004; McGowan *et al.*, 2011; Rulli *et al.*, 2005; van Steensel *et al.*, 2005) made possible to further delineate the clinical phenotype in both sexes, and to exclude an X-linked recessive transmission, previously considered since the absence of female cases (Bruglen *et al.*, 2003; Titomanlio *et al.*, 2001).

1.2 Differential diagnosis of Myhre syndrome

Overlapping syndromes create diagnostic difficulties and, before discovery of molecular causes of these clinical conditions, the lack of knowledge of MYHRS and related disorders genetics increased the complexity of medical diagnosis. Clinical features of MYHRS are known to overlap with features of Moore-Federman syndrome (MIM 127200), GOMBO syndrome (MIM 233270), stiff skin syndrome (MIM 184900), acromicric dysplasia (AD, MIM 102370), Weill-Marchesani syndrome (WMS1, MIM 277600; WMS2, MIM 608328), geleophysic

dysplasia (GPHYSD1, MIM 231050; GPHYSD2, MIM 614185) and LAPS (Laryngotracheal Stenosis, Arthropathy, Prognathism, and Short Stature, MIM 603391). In 1989, Verloes and co-workers reported a brother and sister and probably a third sib with a characteristic recessive inherited phenotype. Patients showed severe microcephaly, brachydactyly with clinodactyly affecting the 5th finger, delayed growth in puberty, and severe mental retardation. Since the similarity between this condition, that they called GOMBO syndrome (Verloes *et al.*, 1989; Verloes *et al.*, 2000), and the one described by Myhre and colleagues in 1981, Bottani and Verloes (1995) suggested that this disorder might be the same as Myhre syndrome.

Stiff skin syndrome, is an autosomal dominant disorder, first described in 1971 in one sporadic and one familial case (Esterly and McKusick, 1971). It is characterized by diffusely hard and thick skin, which limits joint mobility and causes flexion contractures (Loeys *et al.*, 2010).

In 1965, Moore and Federman described six members of three generations of a family. Patients displayed short stature, stiff joints, ocular abnormalities (hyperopia, glaucoma, cataract, retinal detachment), asthmatic bronchitis and hepatomegaly. Authors called this clinical phenotype as familial dwarfism associated with "stiff joints", which showed an autosomal dominant pattern of inheritance. Several major features of Moore-Federman syndrome are shared by acromicric dysplasia (AD) patients.

First reported in 1986 by Maroteaux and collaborators, acromicric dysplasia displays an autosomal-dominant mode of inheritance and its clinical synopsis includes, as well as for Moore-Federman syndrome, short stature, joint limitations, and skin thickening. Since overlapping features, was postulated that these two syndromes may be the same condition (Winter *et al.*, 1989). Nevertheless, acromicric dysplasia is characterized by peculiar traits, such as distinctive facial features (a round face, well-defined eyebrows, long eyelashes, a bulbous nose with anteverted nostrils, a long and prominent philtrum, and thick lips with a small mouth), hoarse voice, pseudomuscular build and distinct skeletal characteristics (including an internal notch of the femoral head, an internal notch of the second metacarpal, and the external notch of the fifth metacarpal). Unlike MYHRS, neither Moore-Federman nor acromicric dysplasia are associated with mental retardation. Further, acromicric dysplasia has some phenotypic overlap with geleophysic dysplasia.

This syndrome was first reported in 1971, and at that time an autosomal recessive inheritance was suggested (Spranger *et al.*, 1971). Beside the radiological features in common with acromicric dysplasia (including delayed bone age, cone-shaped epiphyses, shortened

long tubular bones, and ovoid vertebral bodies), affected individuals show a characteristic facies ('happy' face with full cheeks, shortened nose, hypertelorism, long and flat philtrum, and thin upper lip), progressive cardiac valvular thickening often leading to an early death, toe walking, tracheal stenosis, respiratory insufficiency, and lysosomal-like storage vacuoles in various tissues.

Weill-Marchesani syndrome (WMS) is a rare connective tissue disorder characterized by short stature, brachydactyly, joint stiffness, and lens abnormalities (Faivre *et al.*, 2002). This syndrome can be differentiated from geleophysic dysplasia and acromicric dysplasia by the presence of dislocation of microspherophakia, an eye lens (crystalline) that is smaller than normal and has rounded shape. This may cause severe myopia, as well as glaucoma and/or cataract (Weill, 1932; Marchesani, 1939). Two modes of inheritance have been reported for WMS: autosomal dominant and autosomal recessive (Meyer and Holstein, 1941).

Moreover, before discovery of genetic variants causing MYHRS, Laryngotracheal Stenosis, Arthropathy, Prognathism, and Short Stature was also considered as a differential diagnosis. In 2002, Lindor and co-workers reported 2 unrelated females both exhibiting short stature, deep-set eyes, midface hypoplasia, prognathism, and sparse, fine hair. They also showed brachydactyly, thickened calvarium, vertebral fusions, progressive diffuse joint stiffness, thickened skin and laryngotracheal stenosis, which required a tracheostomy in both patients as young adults. Despite the partially overlapping features with MYHRS, this disorder was described as a separate entity based on the presence of a recurrent laryngotracheal stenosis. Authors proposed the eponym LAPS for this syndrome, to reflect the most consistently recognized features (laryngotracheal stenosis, arthropathy, prognathism, and short stature). However, the similarity between MYHRS and LAPS, particularly the short stature, progressive joint limitation and the facial anomalies, made Lindor postulate that they could represent variable expressivity of the same entity (Lindor, 2009).

1.3 Molecular bases of acromelic dysplasias

Weill-Marchesani syndrome, geleophysic dysplasia, acromicric dysplasia and Myhre syndrome are now ascribed to the acromelic dysplasia group, which is characterized by short stature, short hands and feet, stiff joint and “muscular” build (Le Goff and Cormier-Daire, 2012). The recognition of molecular causes of WMS, GD and AD allowed the identification of

the cellular pathway involved in this phenotypic class, suggesting that variants in other interactors of the same signaling network could produce clinically-related conditions.

In 2003, Faivre and colleagues identified mutations in *Fibrillin 1* (*FBN1*) in the autosomal dominant form of Weill-Marchesani syndrome (WMS1), and in 2004 Dagoneau and coworkers showed that *ADAM metallopeptidase with thrombospondin type 1 motif 10, (ADAMTS10*) is the gene mutated in the autosomal recessive form of the same disorder (WMS2). *FBN1* encodes for an extracellular matrix glycoprotein that serves as a structural component of 10-12 nm calcium-binding microfibrils. These microfibrils provide force bearing structural support in elastic and non-elastic connective tissue throughout the body. ADAMTS10 was recently proved to promote FBN1 deposition in extracellular matrix of cultured fibroblasts, supporting a role of this ADAM protein in microfibril biogenesis (Kutz *et al.*, 2011). As pointed out by a clinical review of 128 WMS patients (Faivre *et al.*, 2003a), does not exist any significant distinctive feature between patients with mutations in one or in the other of the two genes. For this reason, WMS appears to be a clinically homogeneous but genetically heterogeneous disorder.

In 2008, studying 5 consanguineous families with geleophysic dysplasia and 1 sporadic case, Le Goff and collaborators identified 4 distinct nonsense and 1 missense mutations in *ADAMTS-Like Protein 2* (*ADAMTSL2*). This gene encodes a secreted glycoprotein that is involved in regulating TGFβ bioavailability (Le Goff *et al*., 2008). *ADAMTSL2* mutations found in these patients, satisfied the autosomal recessive mode of inheritance previously reported for this syndrome. However, the absence of *ADAMTSL2* mutations in 19 out of 33 geleophysic dysplasia patients involved in the study suggested genetic heterogeneity.

In 2011, performing exome sequencing on 5 cases and then testing candidate variants on a larger cohort, Le Goff and coworkers identified heterozygous *FBN1* mutations in 19 geleophysic dysplasia and 10 acromicric dysplasia affected cases. While geleophysic dysplasia has been initially described as an autosomal recessive disorder, the identification of heterozygous mutations in *FBN1* demonstrated the presence of a geleophysic dysplasia dominant form (GPHYSD2), which strictly fulfills the diagnostic criteria of the recessive form (GPHYSD1) (Le Goff *et al.*, 2012). Since GPHYSD2, AD and the dominant form of WMS (WMS1) are all caused by heterozygous *FBN1* mutations, these disorders are considered as clinically distinct but allelic conditions.

These molecular findings pointed out the crucial role of the transforming growth factor beta (TGFβ) signaling dysregulation in the pathogenesis of acromelic dysplasia disorders (Fig. 1).

In Table 1 the main distinctive features and patterns of inheritance of WMS, acromicric dysplasia and geleophysic dysplasia are summarized.

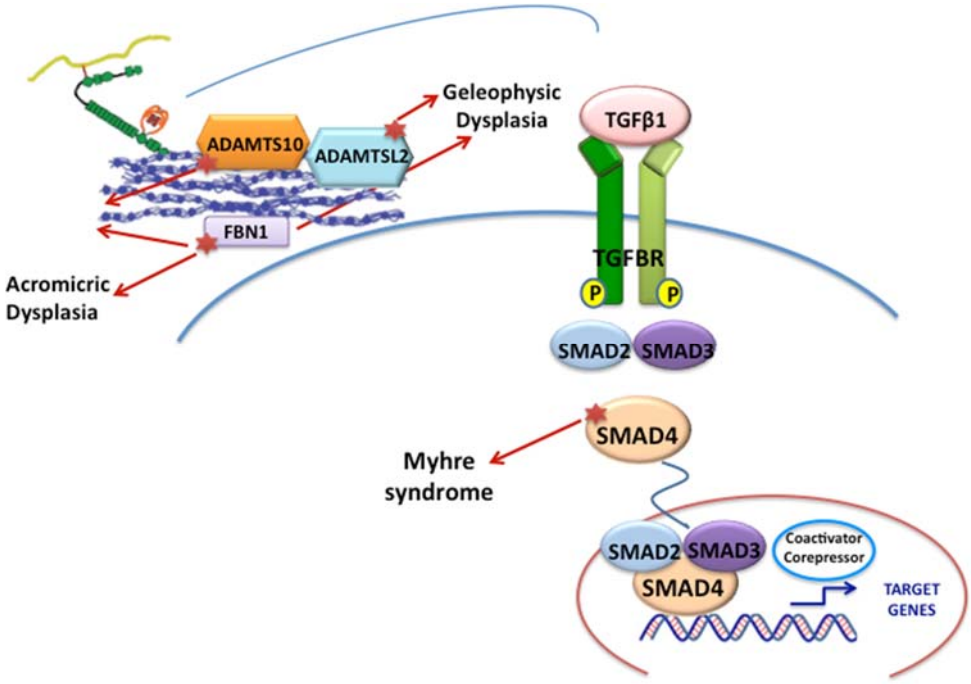

Figure 1: Schematic representation of the proteins involved in the TGFβ signaling that are mutated in acromelic dysplasias.

Table 1. Mode of inheritance, causative genes, OMIM references and principal distinctive traits of Weill-Marchesani syndrome, acromicric dysplasia, geleophysic dysplasia and Myhre syndrome (modified from Michot *et al.*, 2014).

	Weill-Marchesani syndrome	Acromicric dysplasia	Geleophysics dysplasia	Myhre syndrome
Mode of inheritance	Recessive/dominant	Dominant	Recessive/dominant	Sporadic
OMIM	MIM 277600/ MIM 608328	MIM 102370	MIM 231050/ MIM 614185	MIM 139210
Gene(s)	ADAMTS10/FBN1	FBN1	ADAMTSL2/FBN1	SMAD4
Main distinctive features	Dislocated lens; microspherophakia	Hoarse voice	Progressive disorder: 1. cardiac valvular thickening 2. respiratory insufficiency 3. liver enlargement 4. early death possible	Deafness; intellectual disability ; behavioral troubles
Facial features	—	Round face; full lips; well defined eyebrows; long eyelashes; bulbous nose with anteverted nostrils; long philtrum; thick lips with a small mouth	Narrow eyes; full cheeks; shortened nose; hypertelorism; long flat philtrum; thin upper lip vermilion	Short palpebral fissures; maxillary hypoplasia; prognathism; short philtrum
Distinctive radiological features		Internal notch of the femoral head and of the 2nd and 5th metacarpal		Thick clavaria; hypoplastic iliac wings; broad ribs; large vartebrae with short and large pedicles

1.4 Molecular basis of Myhre and LAPS syndromes

1.4.1 Myhre causative mutations

In 2011, to identify the disease gene underlying MYHRS, Le Goff and our research groups independently and simultaneously applied the new strategy of Whole Exome Sequencing (WES) to two and a single affected individual, respectively, with phenotypic characteristics fitting MYHRS. Based on the evidence that all affected subjects were born to apparently healthy non consanguineous parents, both groups considered heterozigosity for a *de novo* mutation as the most likely event causing this disorder. Among variants detected by using exome sequencing approach, both groups considered the novel heterozygous missense changes affecting *mothers against DPP homolog 4* (*SMAD4*) gene as the most promising candidate, given SMAD4 crucial role in BMP/TGFβ signaling and its ubiquitous expression. Gene scanning for mutations in DNA from additional affected patients confirmed the causal involvement of *SMAD4* in MYHRS. Le Goff and collaborators identified 5 patients with A to G change in coding position 1498 (c.1498 A>G, NM_005359; p.Ile500Val; NP_005350), 5 patients with T to C change in coding position 1499 (c.1499T>C, p.Ile500Thr), and 1 patient with A to G change in coding position 1500 (c.1500A>G, p.Ile500Met) in their cohort of 11 subjects. Among our 8 patients, 5 shared the c.1498 A>G nucleotide change (p.Ile500Val), whereas the c.1499T>C change (p.Ile500Thr) was identified in the 3 remaining patients.

The Ile500 residue is located in the MAD homology 2 (MH2) domain, a region at the C-terminus of the protein that is conserved among *SMAD4* orthologs and paralogs. In agreement with its role of tumor suppressor, germline loss-of-function mutations in *SMAD4* are known to cause two cancer-prone diseases, that are the juvenile polyposis syndrome (JPS, MIM 174900) and JPS hereditary hemorrhagic telangiectasia (JPS-HHT), (Gallione *et al.*, 2004; Gallione *et al.*, 2010). Further, somatic intragenic lesions or *SMAD4* gene deletions frequently occurs in carcinomas of the pancreas, gastrointestinal tract and skin. Despite this, no missense mutation affecting Ile500 were previously reported in human disease, supporting the idea that the narrow spectrum of *SMAD4* Myhre mutations has distinct and specific consequences on *SMAD4* function (Fig. 2).

After *SMAD4* discovery as the gene causing Myhre syndrome, Lindor and co-worker tested their LAPS cases (Lindor *et al.*, 2012) for *SMAD4* coding sequence, and identified the same

mutations described by Le Goff and Caputo in Myhre syndrome patients (c.1499T>C, p.Ile500Thr; c.1498 A>G, p.Ile500Val). This finding suggested that Myhre and LAPS are the same entity, and redefined the phenotype for this syndrome.

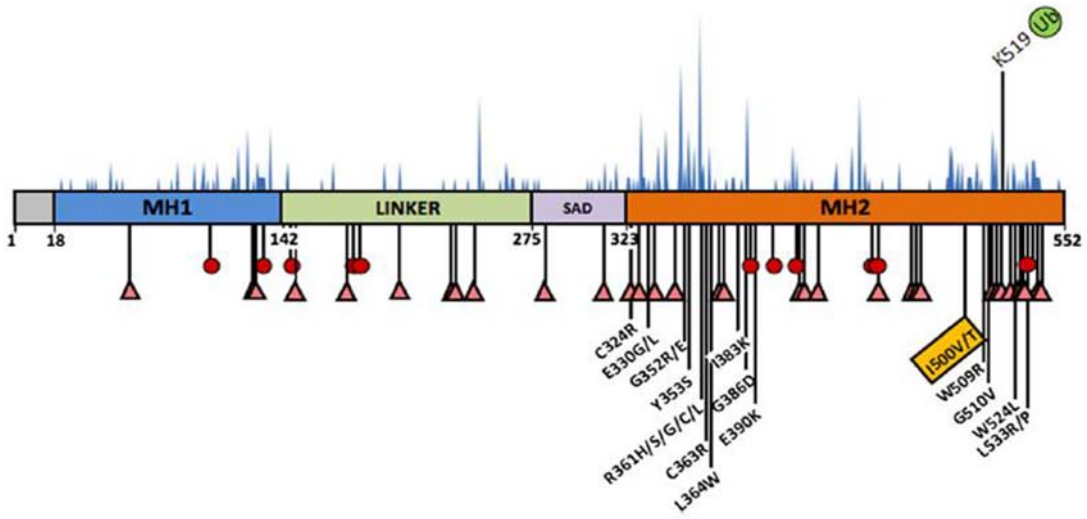

Figure 2. A restricted spectrum of germline missense mutations in *SMAD4* underlies Myhre syndrome. The location of Ile500 (yellow label) is shown below the SMAD4 domain structure scheme. SMAD4 comprises an N-terminal MAD homology 1 domain (MH1) connected by a linker to the SMAD4 activation domain (SAD) and the C-terminal MAD homology 2 domain (MH2). Numbers below the domain structure indicate the amino acid boundaries of those domains. The distribution of somatic SMAD4 mutations occurring in cancer (blue-filled peaks) is shown above the illustration. The location of Lys519, which is the residue subject to ubiquitination, is also shown. JPS and JPS-HHT nonsense (red circle) and truncating (pink triangle) causative mutations are found throughout the gene, supporting a loss of function model of action. (from Caputo *et al.*, 2012)

1.4.2 SMAD4 protein function and Isoleucine 500 variants structural analysis

SMAD4 encodes a protein belonging to the 8-member family of SMADs, which is divided into 3 functional classes: the receptor regulated SMADs (R-SMADs: SMAD1, SMAD2, SMAD3, SMAD5 and SMAD8), the inihibitory SMADs (I-SMADs: SMAD6 and SMAD7) and the co-mediator SMAD (Co-SMAD, that in human is SMAD4), (Attisano *et al.*, 2001). Smad transcription factors lie at the core of the transforming growth factor-β (TGFβ)/BMP signaling network, that regulates a vast array of biological processes, including cell proliferation, differentiation, apoptosis, migration, adhesion, extracellular matrix production, angiogenesis, immunity and development (Massagué *et al.*, 2000). Within this signaling network, SMAD4 represents a central node, because it is required as a coactivator to have transcriptionally active SMAD complexes (Massagué, 1998; Massagué *et al.*, 2005).

The TGFβ /activin and BMP subfamilies of cytokines, belonging to the TGFβ superfamily, act through the TGFβ/BMP pathway binding to pairs of TGFβ receptor 1 (TGFBR1) and TGFβ receptor 2 (TGFRB2) membrane receptor serine/threonine kinases, promoting the formation of a hetero-tetrameric receptor complex. Phosphorylation of the regulatory region GS domain on TGFBR1 by TGFRB2 creates a repeated pS–x–pS motif that serves as a docking site for RSmads. TGFBR1-mediated phosphorylation at the C terminus of RSmads creates a pS–x–pS motif, allowing the dissociation of phosporilated R-SMADs from the receptor, their accumulation in the nucleus and the recognition of this motif by a basic pocket in SMAD4. R-SMADs form heterodimers with SMAD4 and the resulting Smad complex incorporates different DNA-binding cofactors that confer target gene selectivity and influence the recruitment of either transcriptional coactivators or corepressors. In this fashion TGFβ controls transcription activation or repression of hundreds of genes (Massagué *et al.*, 2005).
The best characterized complexes formed by SMAD4 are those resulting from its association with SMAD2 (MIM 601366) or SMAD3 (MIM 603109). Biochemical and crystallographic evidence indicates that these complexes are trimeric units comprising one SMAD4 and two phosphorylated R-SMAD subunits. According to these crystal structures, Ile500 is located within one of the two MH2 surfaces involved in R-SMAD binding, and the residues surrounding it (particularly Arg497 and Asp493) directly participate in the intermolecular interaction. Structural analysis, performed in collaboration with Prof. Bocchinfuso e Prof. Stella from Tor Vergata University (Fig. 3) showed that substitution of Ile500 by Threonine or Valine in SMAD4 could affect the proper function of the SMAD heterotrimer. It was also speculated that these amino acid changes might improper correct SMAD4 ubiquitination, which occurs at Lysine 519 and controls pathway inhibition (Caputo *et al.*, 2012). The latter hypothesis is also supported by Le Goff immunoprecipitation assay and protein blot analysis, that found decreased ubiquitination of SMAD4 in MYHRS proband cells (Le Goff *et al.*, 2011a).

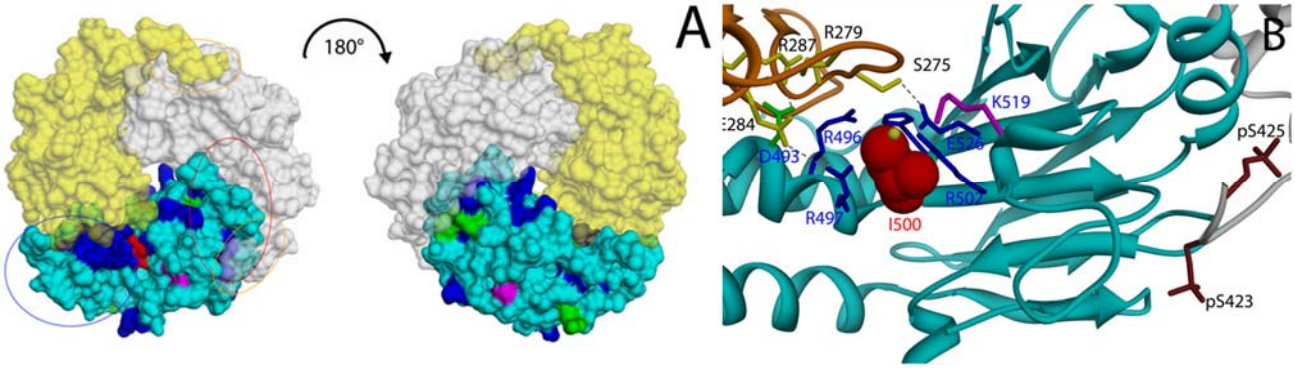

Figure 3. Location of Ile500 in the Spatial Structure of the SMAD3/SMAD4 MH2 Domain Complex (from Caputo *et al.*, 2012).

(A) Solvent accessible surface representation of the SMAD4/SMAD3 MH2 domain complex (Protein Data Bank [PDB] ID codes1U7F). The SMAD4 monomer is shown in cyan, whereas the two SMAD3 subunits are colored in yellow and white. The solvent accessible surface of residues affected by somatic (blue) and germline (magenta) mutations and lesions occurring as both germline and somatic events (green) are shown. The residue mutated in Myhre syndrome, Ile500, is shown in red. The red and blue ovals indicate the location of the loop/helix and helix bundle SMAD4 subdomains, respectively. Orange ovals indicate the position of the serine residues that are phosphorylated in activated SMAD3.

(B) Ca ribbon trace (PDB ID codes 1U7F) of SMAD4 MH2 domain (cyan) and those of the two interacting SMAD3 subunits (orange and gray). Ile500 is represented in space-filling mode (red). Residues interacting with Ile500 (Arg496, Arg497, Arg502, Glu526, and His528) are shown as blue sticks. Asp493 (green), which is important for interdomain interactions, and Lys519 (violet), which is subject to ubiquination, are also shown. SMAD3 residues directly contributing to interactions with the evidenced SMAD4 residues (Ser275, Arg279, Glu284, and Arg287) are shown as yellow sticks, together with the phosphorylated SMAD3 serine residues (brown). The anion binding site located in proximity of Ile500, as indicated by the structure of the SMAD4 homotrimer (pdb code 1DD1), is shown by a yellow sphere. Visualization and analysis of the molecular structure was performed with the program UCSF Chimera (Pettersen *et al.*, 2004).

1.4.3 MYHRS clinical features: an update

Since molecular bases discovery, other MYHRS patients harboring mutations in *SMAD4* were reported, better characterizing the phenotypic spectrum of this disorder (Asakura *et al.*, 2012; Al Ageeli *et al.*, 2012; Hawkens and Kini, 2015; Ishibashi *et al.*, 2014; Piccolo *et al.*, 2014; Picco *et al.*, 2013; Starr *et al.*, 2015). A comprehensive review of MYHRS affected patients have been recently published by Michot and collaborators. A total of 32 unrelated patients with MS or LAPS diagnosis, 17 of whom had been previously described, were recruited in the study. Among them, 29 have a *SMAD4* mutation, including the two patients with LAPS syndrome reported by Lindor and 3 cases had no mutation in the *SMAD4* coding sequence. In Table 2 and Figure 4 clinical findings of these patients are shown. All the canonical features of Myhre syndrome were consistently observed among all cases. Indeed, progressive thickness of the skin was found in all but 2 patients (30/32, 94%), muscular pseudohypertrophy was present in 31 on 32 cases (97%), and all patients had joint limitation, either of small joints (26/32, 81%) or of large joints (27/32, 84%). Among facial dismorphisms, most common consisted of short palpebral fissures, mid-face hypoplasia, short philtrum, prognathism, narrow mouth and small ears. Each one of these features has been observed in 24–27/32 cases (77-84%).

Other frequently associated signs are listed below: intrauterine growth retardation was observed in 23/29 (79.3%) cases, postnatal growth retardation, ranging from_2SD to _5.5SD was present in 22/32 (68,7%) cases, all patients except one (31/32, 96.8%) had small hands and feet, intellectual disability was reported in 28/32 (87.5%) patients ranging from mild to moderate, except for one case who had severe disability, impairment of speech development was present in 22/32 (68,7%) patients, behavioral disorders were frequently reported (18/32, 56%) and consisted of a wide range of problems, including hyperactivity, stubbornness, aggressiveness, frustration, intolerance, poor communication skills, autistic features and polyphagia, hearing loss, predominantly conductive or mixed, was frequently reported, affecting 25/32 (78%) patients.

Interestingly, the two LAPS patients also present with the same gestalt as all other patients. The laryngotracheal stenosis, which led to the description of the LAPS entity, was also observed in 3 Myhre cases. These findings clearly support the homogeneity of this syndrome and the view that Myhre and LAPS syndromes are phenotypic variants of the same disorder.

Table 2. Clinical and radiological features of 17 female and 15 male patients affected by MYHRS reviewed in Michot *et al.*, 2014.

Diagnosis	SMAD4 Affected residue	Paternal age at birth (average)	General					Main features		
			Sex	IUGR	Height range	Overweight	Microcephaly	Intellectual deficency	Muscular hypertrofy	Tickened skin
MS 28/32 LAPS	I500 30/32 R496 2/32	36.7	F 17 M	20/26	-6 to +2	11/25	3/26	28/32	32/32	30/32

Facial features							
Short PF	Ptosis	Mid-face hypoplasia	Short philtrum	Prognathism	Narrow mounth	Thin upper lip	Small ears
27/32	6/31	25/32	24/32	26/32	25/32	19/31	24/31

Radiological features						
Brachydactily	Thick femoral neck	Platyspondyly	Large pedicles	Narrow pelvis	Broad ribs	Thick calvaria
18/23	10/17	6/15	11/18	8/17	8/18	13/19

Long-term complications							
Hearing loss	Strabismus	Refractory abnormalities	CHD	Hypertension	Recurrent infections	Intestinal/renal abnormalities	Abnormal puberty
25/32	10/29	13/28	17/31	9/30	17/29	8/28	9/29

Abbreviations: LAPS, laryngotracheal stenosis, arthropathy, prognathism and short stature syndrome; IUGR, intrauterine growth retardation; PF, palpebral fissures; --, no mutation identified. Other long term complications include

cataract (3/32), respiratory insufficiency (7/27). All the reported patients are sporadic cases. No familial transmission has been reported so far.

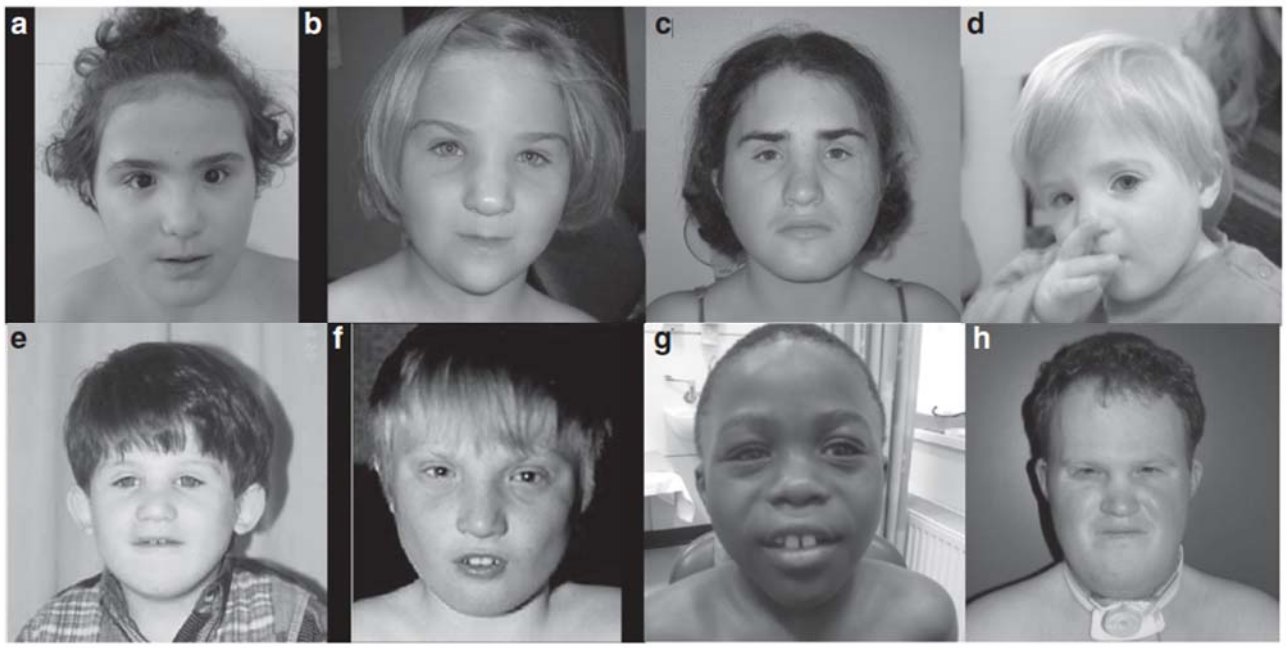

Figure 4 (a-h). Distinctive facial features of representative MYHRS subjects carrying the heterozygous Ile500 mutations (from Michot *et al.*, 2014).

1.4.4 Contribution of advanced paternal age to the origin of punctiform mutations

Studies of mutations in humans have long established that there is a gender-specific signature in the origin of different types of genetic alterations (Goriely and Wilkie, 2012). Although chromosomal non-disjunctions originate mainly in the female germline and large genomic rearrangements might show either a male or a female bias in origin, the majority of point mutations and small deletions or insertions tend to be paternal in origin. This gender bias is generally explained by fundamental differences in germ cell biology in the female and in male lineages (Fig. 5). By the time of birth, germ cells in the developing ovary have already completed their proliferative phase. In fact, oocytes are arrested in prophase of meiosis I until sexual maturity, when one oocyte per month is selected to resume the cell cycle (Crow, 2000). Because of more cell divisions over a prolonged period during spermatogenesis compared to oogenesis, the mutation rate for single-*locus* mutations is higher in men then in women and increases with paternal age (Crow, 1997).

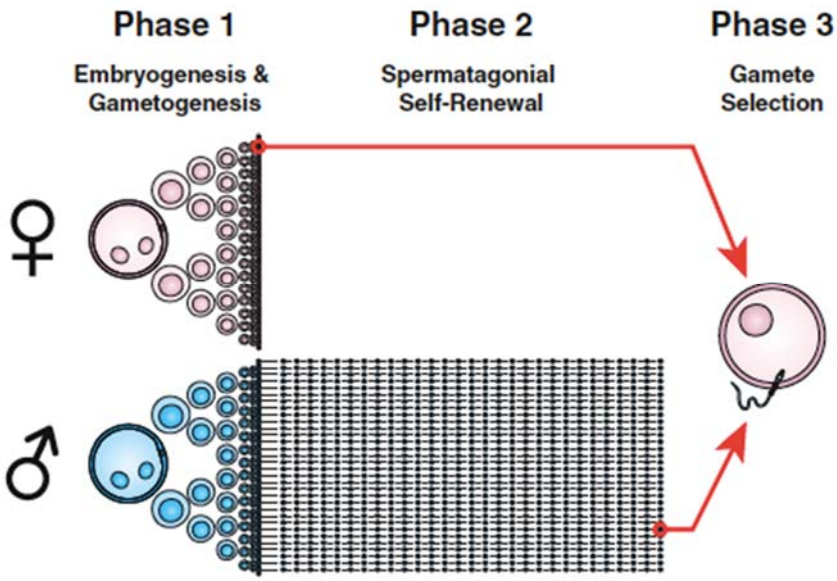

Figure 5. Stochastic-Process Model of Sexual Dimorphisms during Gametogenesis (from Campbell *et al.*, 2014).
Phase 1: both males and females experience a stochastic exponential cell-expansion phase modeling embryogenesis and germ cell proliferation. Mutations can arise in any cell division, and if they persist in the clonal lineage, they could ultimately be available to be transmitted to the next generation.
Phase 2: in males, expansion is followed by a stochastic but nonexpanding self-renewal process modeling spermatogenesis.
Phase 3: a single sperm and egg are randomly sampled after meiosis to fertilize an offspring.

Although in some cases the association between advanced paternal age and genetic disorders is controversial, the situation is very different for a small group of congenital diseases, named "paternal age effect" (PAE) disorders. These spontaneously arising dominant genetic disorders, such as achondroplasia, Apert, Noonan, Costello syndromes and multiple endocrine neoplasia type 2A and 2B (Goriely and Wilkie, 2012), are caused by specific gain-of-function mutations in fibroblast growth factor receptors (FGFRs), other tyrosine-kinase receptors, and components of the RAS/mitogen activated protein kinase (MAPK) signaling pathway. The apparent high mutation rates at specific genomic sites that give rise to paternal age effect conditions, and the age-related effect, are best explained by a phenomenon termed selfish spermatogonial selection. Mutations arising by chance at key positions in PAE genes during spermatogonial stem cells (SSCs) divisions are associated with gain-of-function properties, conferring a proliferative or survival advantage on the mutant SSC. This leads to expansion of the mutant clone over time in a manner similar to oncogenesis, resulting in increased levels of mutant spermatozoa (Maher *et al.*, 2014). This phenomenon, combining hypermutability of specific nucleotides, expression of this mutant in spermatogonial stem cells and further

positive selection resulting in localized clonal expansion, has been demonstrated for recurrent mutations of *FGFR2* and *FGFR3* genes in Apert syndrome and achondroplasia (Michot *et al.*, 2014).

All MYHRS *SMAD4* mutations identified occured *de novo* and no familial transmission has been reported so far. The high average paternal age at birth, confirmed by the last reviewed data (36.7 years), combined with the prevalence of Ile500 change due to mainly two nucleotides changes in *SMAD4*, may suggest a mechanism of protein-driven selfish selection in sperm.

2. Aim of the study

The main purpose of this PhD project has been the investigation of the molecular bases of Myhre syndrome. To reach this goal, we used different approaches (functional and *in silico*) in order to characterize this syndrome. Since *SMAD4* discovery as the gene mutated in MYHRS, we performed several cellular assays, in order to assess MYHRS mutations functional impact on SMAD4 protein localization, expression, and on cell proliferation. Moreover, in order to characterize the phenotypic spectrum of MYHRS mutations and perform genotype-phenotype correlations, we collected a cohort of cases that showed clinical features fitting MYHRS and screened them for *SMAD4* coding sequence.

Finally, in view of the fact that many spontaneous dominant disorders caused by point mutations tend to display a paternal origin, we performed the investigation on the parental germline origin of MYHRS-causing mutations.

3. Materials and Methods

3.1 Functional characterization of MYHRS Ile500 variants

To explore *SMAD4* MYHRS mutations functional impact, three distinct approaches were carried out. Firstly, we evaluated SMAD4 expression in fibroblasts from patients and in transiently transfected HeLa cells. Furthermore, we investigated protein localization in patients' fibroblasts, by immunofluorescence and confocal laser microscopy analysis. Moreover, since SMAD4 plays a role in cell proliferation, we evaluated cell growth by growth

curve analysis in fibroblasts from patients and by BromodeoxyUridine (BrdU) incorporation assay in both patient fibroblasts and transiently transfected 3T3 fibroblast cell line.

3.1.1 SMAD4 constructs and transfection

For SMAD4 overexpression in HeLa and 3T3 cells, we performed transient transfection of pcDNA6-Xpress SMAD4 constructs (WT, Ile500Val, Ile500Thr). Mutant *SMAD4* coding sequence (CDS) was obtained performing direct mutagenesis, by using Site direct mutagenesis kit (Stratagene). Constructs were produced subcloning WT and MYHRS-mutated *SMAD4* CDS in pcDNA6-Xpress tagged vector, by using BamH1 and Xho1 restriction enzymes (New England Biolab). Constructs (3 μg/each) were transfected by incubating with FuGENE® 6 Transfection Reagent (Promega) in DMEM High for 15 minutes at room temperature, and then adding dropwise Transfection Reagent/DNA mixture to HeLa cells at 60-70% confluence, swirling gently.

3.1.2 Cell culture and TGFβ treatment

Skin biopsies were obtained from 2 MYHRS cases (TO_01 and NA_01) with Ile500Thr and Ile500Val variants respectively, while control wild-type fibroblasts were obtained from a healthy subject (ATCC). HeLa and 3T3 cell lines were supplied by ATCC. Primary fibroblasts as well as cell lines were cultured according to standard procedures in DMEM High (Euroclone) with 10% Fetal Bovine Serum (FBS) and penicillin/streptomycin, in a humidified atmosphere containing 5% CO_2 at 37°C. For SMAD4 expression assay, a TGFβ (2,5 ng/ml, Peprotech) treatment on HeLa cells 24 hours post-transfection was performed for 1 hour. To evaluate SMAD4 mutants localization, the same treatment was carried out on affected and WT fibroblasts, for 1, 2.5, and 5 hours.

3.1.3 SMAD4 expression: Western blot analysis of MYHRS fibroblasts and HeLa cells

To assess MYHRS-mutated SMAD4 expression at cellular level, Western blot analysis of primary fibroblasts and HeLa transiently transfected cells was performed. Two days cultured

primary fibroblasts and 24 hours post-transfection TGFβ stimulated HeLa cells, were respectively collected and proteins were extracted in Marais lysis buffer (25mM Hepes pH 7.8, 400 mM KCl, 5 mM EDTA pH 8, 0,4% NP4O, 10% Glycerol), supplemented with 1mM Dithiothreitol, protease (complete mini protein inhibitor cocktail, Roche Diagnostics) and phosphatase (phosphostop, Roche) inhibitors. After centrifugation at 4°C at 13 000 rpm for 30 min, protein lysates were quantified by spectrophotometer (Thermoscientific) and immediately boiled in SDS sample buffer. Thirty µg of purified proteins were separated by 10% polyacrylamide gel (Bio-Rad). Protein blot was performed by using Trans Blot Turbo Transfer System and Transfer Pack (Bio-Rad), applying provided protocol. Anti-SMAD4 (1:250, Santa Cruz, SC-7154) monoclonal antibody was used to detect endogenous SMAD4 proteins from control and MYHRS samples. GAPDH detected by anti-GAPDH antibody (1:250, Sigma-Aldrich, G9545) was used to normalize protein content for each sample. Ectopic SMAD4 protein was revealed by immunoblot with primary anti-Xpress (1:1000, Life Technologies, R91025) antibody. Protein expression was assessed by normalizing either SMAD4 or Xpress band intensity with respect to endogenous GAPDH. The results were confirmed in three independent experiments. Optical density measurements of Western blot bands were performed with the ImageJ software.

3.1.4 SMAD4 localization: immunofluorescence analysis and confocal laser scanning microscopy

MYHRS Ile500Thr and Ile500Val patients and control fibroblasts were seeded on 8 wells chamber slides (Nunc Lab-Tek, 177445). 24 hours post-seeding, TGFβ treatment was performed. Next, treated and untreated cells were PBS washed, fixed in 4% paraformaldehyde for 30 min at 4°C, and washed again. Subsequently, cells were quenched with NH_4Cl for 10 minutes at room temperature. After 10 minutes permeabilization with 0.5% Triton X-100 at room temperature, cells were PBS washed and then incubated 1 hour at 37°C with 5µg/ml rabbit anti-SMAD4 primary antibody. Then, cells were washed again and incubated for 1 hour at 37°C with 5 µg/ml anti-rabbit Alexa Fluor®568 secondary antibody (Life Technologies) and washed twice. After 30 minutes incubation with Alexa Fluor®488-Phalloidin (Life Technologies), coverslips were washed and then mounted on glass slides with 5 µg/ml Dapi (Life Technologies) nuclear dye in anti-fade reagent (Life Technologies) and analyzed. Imaging was performed on an Olympus FV1000 apparatus, utilizing excitation spectral laser

lines at 405, 488 and 561 nm. Signals from different fluorescent probes were taken in sequential scanning mode.

3.1.5 Cell proliferation: growth curve and BrdU incorporation assay

Since SMAD4 regulates proliferation, we also tested the effect of MYHRS-mutated SMAD4 on cell growth. To this goal, two distinct proliferation assays were performed. Firstly, for control and affected fibroblasts growth curve was calculated. Cell number was counted at 3, 6 and 9 days of culture by a using Bürker chamber, with standard protocol (cells were trypsinized and resuspended in standard medium; an aliquot was counted under a Nikon inverted optic microscope). Secondly, BrdU incorporation assay was carried out on both patients and WT control fibroblasts, as well as on 3T3 SMAD4-transfected cells. Cells were seeded on 8 well chamber slides. Transfection of 3T3 cell line and cell cultures were performed as described before. After a BrdU pulse (50microM, Sigma-Aldrich) of 5 hours at 37°C, cells were PBS washed twice, fixed with PFA for 20 minutes at room temperature, and washed again. After 10 minutes permeabilization with 0.2% Triton X-100 in Washing Buffer (WB, 0.3% BSA in PBS) at room temperature, cells were washed in WB and then incubated with DNAse (Sigma-Aldrich) for 45 minutes at 37°C in humidified chamber. After that, cells were washed with 0.2% Tween-20 in WB and incubated 1 hour at 37°C with 5µg/ml mouse anti-BrdU primary antibody (BD biosciences). Then, cells were washed with WB and stained for 1 hour at 37°C with anti-mouse Alexa Fluor 568 secondary antibody (Life Technologies). Finally, slides were washed twice in WB and once in PBS-and coverslips were mounted on chamber slides with 5 mg/ml DAPI nuclear dye in anti-fade reagent and analyzed. Immunofluorescence analysis of BrdU incorporation was performed using a fluorescence microscope (Nikon).

3.2 MYHRS samples collection

After *SMAD4* identification as the gene mutated in MYHRS, we collected samples of other 14 cases with Myhre syndrome clinical diagnosis, and, in some cases, with characteristics partially fitting the syndrome main features. These patients were examined in several hospitals by clinical geneticists, which provided biological samples and clinical details. We received MYHRS cases to test for *SMAD4* variants from Università di Torino (2 cases), Newcastle University (1 case), Zurigo University (1 case), Università di Napoli (4 cases),

Ospedale Fatebenefratelli (1 case), Ospedale S. Camillo-Forlanini (1 case), Washington University (1 case), Kuala Lumpur Hospital (1 case), and University of Alexandria (2 cases). Among these patients, some presented phenotypic variability just partially overlapping the MYHRS typical appearance; others exhibited all the classic features of the syndrome. After *SMAD4* screening, Whole Exome Sequencing (WES) approach was applied to a selection of *SMAD4* mutation negative patients: data analysis is still in progress. Clinical data and collection of biological material have been obtained in agreement with ethical standards of institutional revision committees and with informed consent.

3.3 Molecular screening of *SMAD4*

SMAD4 mutation analysis was performed for all of these patients. DNA was extracted from whole blood samples of cases and parents by using *Purgene DNA isolation Kit* (Gentra), with relative standard protocol. After primers design (Table 3) and PCR amplification of the 11 coding exons of the gene using GoTaq polymerase (Promega, see protocol details reported in Table 4), specificity of amplification was tested performing 2% agarose gel electrophoresis. After PCR products purification, performed by using NucleoSpin Gel and PCR Clean-up (Macherey-Nagel) with standard conditions, Sanger sequencing of purified PCR products was carried out, by using ABI BigDye Terminator Cycle Sequencing kit v. 3.1 (Applied Biosystems, protocol details are reported in Table 5) and an ABI Prism 3500 Genetic Analyzer (Applied Biosystems). Sanger sequencing purification was performed by using MSB Vario Cleanup (Stratec molecular), applying standard protocol. Then, *SMAD4* electropherograms analysis was performed by using ChromasPro (Technelysium Pty Ltd) and Sequencing Analysis Software v.5.4 (Applied Biosystems), taking GeneBank NG_013013.2 as reference sequence, in order to detect mutations eventually localized in this gene. Information on annotation and allele frequency of identified variants was retrieved from population databases (e. g. dbSNP and ExAC). In mutation positive cases, amplification and Sanger sequencing of DNA of both parents for the relevant exon was performed, to confirm the *de novo* origin of the variant. Paternity was tested for *SMAD4* mutated patients performing STR Genotyping, by using AmpF*l*STR Identifiler Plus PCR Amplification Kit (Applied biosystems), with producer protocol. Finally, if other patient biological samples were available, extraction of genomic DNA from additional tissues, amplification and Sanger sequencing of the relevant exon were carried out, in order to confirm the germline origin of the mutation.

Table 3. Primer sequences, annealing temperatures and amplicon length for *SMAD4* coding sequence. Forward or Reverse primer for each amplicon were used to perform Sanger sequencing.

Primers and annealing temperature for SMAD4 exons amplification			
SMAD4 exons	Primers sequence	Tann (°C)	Amplicon length (bp)
Exon 1	F GTTTTTCACTGTTTCCAAAG R AATTACCCTGTAGTAGCTTG	58	416
Exon 2	F TGAGTTGGTAGGATTGTGAG R TTGAAACACTATTGAGATCC	58	329
Exon 3	F GATAGCGTTTATGCTACTTC R TTGTTAATGTTACTGCCTGC	58	282
Exon 4	F CACTGTAATTGATTTTAGGTG R GACTACACATAAATAAGCAATG	58	386
Exons 5-6	F AGTTACACTTTTTGCCCATC R AAAAACAGAAAACAAAGCCC	58	526
Exon 7	F AGCACTTGGCAGATAGCACTG R TGTACTCATCTGAGAAGTGACC	60	389
Exon 8	F GCAAGTGAAAGCCTTATATC R GTACATGGGAAAACATAACC	58	330
Exon 9	F AGCTATCTTTTGGTTTTATG R CAACAAATAGAGCTTTAAGTC	58	347
Exon 10	F AATTCTTTTCATGTGAGAGG R ATGCAAACAGGGTCATAGGC	58	445
Exon 11	F ACTTCTTGGCACTTTAGCAGAG R TGTCTGCTAGGAGCAAGGCAG	62	505

Table 4. PCR protocol used for *SMAD4* exons amplification with GoTaq G2 Flexi DNA polymerase.

	Final concentration
DNA	50-100 ng
GoTaq G2 Flexi DNA polymerase	1,3 U
GoTaq Flexi Buffer	1X
MgCl2 solution, 25mM	1,5 mM
Upstream primer	1µM
Downstream primer	1µM
PCR Nucleotide Mix, 10mM each	0.2 mM each dNTP
ddH2O	up to final volume of 30µl

Table 5. Sanger sequencing protocol used for *SMAD4* exons sequencing with Big Dye 3.1.

	Final concentration
DNA	15 ng/100 bp of purified PCR product
Big Dye 3.1 Master Mix	1x
Buffer BigDye terminator [ABI Cycle Sequencing Kit v. 3.1 (Applie Biosystem)]	1x
Upstream or Downstream primer	3.25µM
ddH2O	up to final volume of 20µl

3.4 Novel *SMAD4* mutation and methylation analysis

We investigated the impact of C to T transition in position 1486 of *SMAD4* coding sequence (c.1486 C>T), as 3 out of 14 MYHRS tested patients presented this novel missense heterozygous mutation that produce an Arginine to Cysteine substitution (R496C). To this goal, we performed *in silico* structural analyses in collaboration with Professors Gianfranco Bocchinfuso and Lorenzo Stella, of Tor Vergata University. Further, we preliminary evaluated methylation status of the CpG dinucleotide in which the novel mutation localized. To this purpose, Hpy99I DNA digestion and public human mutations and methylation databases interrogation were carried out.

3.4.1 Structural analysis

Analyses were performed on available crystallographic structures of SMAD heterotrimers (SMAD4/SMAD2, pdb code 1u7v; SMAD4/SMAD3, pdb code 1u7f). For the other SMAD complexes (i.e., SMAD4/SMAD1, SMAD4/SMAD5, and SMAD4/SMAD9), structures were obtained by homology modeling by means of Swiss Model (Arnold *et al.*, 2006), starting from the structure of the SMAD4/SMAD3 complex. The residues of R-SMADs in contact with Arg496 were determined by considering the residues within minimal distance, less than or equal to 4 Å. The coordinates of the Cα and Cβ atoms of the residues Arg496, Arg497, Arg502, Glu526, His528, extracted from the SMAD4 homo-trimer structure (pdb code 1dda, chain A), were used to search for similar structural motifs in other proteins. Rasmot-3D Pro server was used to identify protein structures possessing a motif of similar residues with similar topology (Magis *et al.*, 2006). In this search, residues with similar physical-chemical properties were considered equivalent, and the maximum acceptable distance between corresponding atoms in the reference and the examined structure was set to 1.2 Å (Caputo *et al.*, 2014).

3.4.2 Analysis of c.1486 Cytosine methylation status

As the c.1486 C>T mutation (which produces the Arginine to Cysteine substitution at protein position 496) consists of a heterozygous Cytosine to Thymine transition in a CpG dinucleotide of *SMAD4* coding sequence, we investigated methylation as a possible driving force

responsible for the onset of this variant. To preliminary evaluate the methylation status of the cytosine in position c.1486, we used a restriction endonuclease methylation sensitive Hpy99I (New England Biolabs), which recognizes a short nucleotide sequence (CGWCG, where W indicates Adenine or Thymine nucleotides) and is blocked by methylation. Genomic DNA obtained from peripheral lymphocytes of 1 patient carrying the heterozygous c.1486C>T transition and 1 unaffected control were Hpy99I-digested overnight at 37°C. The sequence corresponding to *SMAD4* exon 11 was PCR amplified and the PCR products were analyzed on a 2% agarose gel. Efficiency of the Hpy99I treatment was confirmed by digestion of the mutant and WT PCR amplified genomic fragments and subsequent visualization of DNA bands on a 2% agarose gel. Expected length for undigested PCR product was 505 bp, whereas those expected for digested amplicon were 184 bp and 326 bp. Methylation DNA assays using sodium bisulfite are ongoing in order to confirm the restriction assay results.

3.4.3 Mutations at *SMAD4* coding sequence CpG dinucleotides and methylation status

In order to evaluate the methylation status of *SMAD4* CpG coding sites, we used in silico approach to retrieve annotations about *SMAD4* CpG dinucletide from distinct human mutation and methylation databases. Firstly, we considered dbSNP (build 141) annotated variants in *SMAD4* CpG sites. dbSNP (Sherry *et al.*, 2001) is a public-domain database that catalogs short genetic variation (that are single nucleotide variations, short nucleotide insertions and deletions, short tandem repeats and microsatellites) of a wide range of species, including human.

Moreover, the ExAC database (version 0.3, http://exac.broadinstitute.org/) was interrogated. The Exome Aggregation Consortium (ExAC) collects exome sequencing data from a variety of large-scale sequencing disease-specific and population genetic projects.

To investigate the pathogenic relevance of described germline and somatic *SMAD4* mutations, Cosmic, OMIM and Clinvar were consulted. COSMIC v75 database (Forbes *et al.*, 2015), that is a catalogue of somatic mutations found in cancer, was consulted in order to retrieve information on somatic cancer-associated variations in *SMAD4* coding sequence CpG sites. The Online Mendelian Inheritance in Man (Hamosh *et al.*, 2005) is a comprehensive catalog of genes and mendelian genetic disorders. Clinvar (Landrum *et al.*, 2014) is an archive of human genetic conditions and associated variations.

Moreover, we evaluated methylation of *SMAD4* coding sequence CpG sites retrieving information from NGSmethDB and MeDIP-seq CpG data. NGSmethDB stored methylation data derived from Next Generation Sequencing (NGS) experiments. (Hackenberg *et al.*, 2011). MeDIP-seq (Methylated DNA immunoprecipitation and sequencing) is a next-generation sequencing-based approach that uses immunoprecipitation to extract the methylated fraction of the genome. (Maunakea *et al.*, 2010). Data retrieved from these databases let us to correlate *SMAD4* annotated variants at CpG sites with the methylation of the mutated cytosine.

3.5 Parental origin of mutations

Genotype and cloning experiments were performed in order to investigate the parental origin of MYHRS mutations.

3.5.1 MYHRS samples collection

A cohort of 16 Myhre syndrome patients with pathogenic *SMAD4* mutations and their parents, were selected. These families were collected from 2011 to date. Among them, 8 were reported in Caputo *et al.*, 2012. Their biological samples and clinical descriptions were provided by several Italian hospitals, that are Ospedale Pediatrico ‘‘Bambino Gesu`’’, Roma; Università di Torino; Arcispedale Santa Maria Nuova; Ospedale Microcitemico, Cagliari; Università ‘‘Federico II’’, Napoli. Other 3 trios were collected subsequently for *SMAD4* mutation screening (from Università di Torino and Ospedale S. Camillo-Forlanini, Roma). 5 *SMAD4*-mutated probands and their parents were provided by Valerie Cormier-Daire group (University of Paris). Clinical data and biological material collection and storage were attained from the participating families in accordance with the ethical standards of the institutional review boards and after written informed consent.

3.5.2 Informative polymorphic sites research

We analyzed these families for the presence of informative polymorphic sites in a 4 kb genomic region flanking Myhre syndrome causative variants. A polymorphism is considered as informative if we are able to identify which of the two parents has transmitted it. DNA was

extracted from whole blood samples of cases and parents by using *Purgene DNA isolation Kit* (Gentra), with relative standard protocol. To search for informative polymorphic sites in the families, we designed 11 overlapping amplicons in order to cover the genomic region encompassing MYHRS variants. We decided to select 4 kb (about 2 kb upstream and 2 kb downstream of MYHRS mutations position) as the maximum extension for informative polymorphisms research, in order to promote the amplification of genomic fragments and minimize the possibility of recombination events. After primer design (Table 6), we performed PCR amplification of proband intragenic fragments and PCR products purification. Sequencing of purified PCR products and electropherogram analyses were then performed, in order to test for the presence in the proband of heterozygosity in a polymorphic site. For those probands resulted heterozygous for a polymorphic site PCR amplification, purification and Sanger sequencing were performed on parental DNAs.

Table 6. Primer sequences, annealing temperatures and amplicon length for *SMAD4* screening fragments. Forward or Reverse primer for each amplicon were used to perform Sanger sequencing.

Primers and annealing temperature for *SMAD4* fragments amplification			
SMAD4 fragments	Primer sequence	Tann (°C)	Amplicon length (bp)
Fragment 1	F ACTGGGATGATGACATTTTTGA R TAGTTTTCTCTCCATGTTTAGC	58	318 bp
Fragment 2	F TTTCAGAATTGGACACTTTTCC R CATATAGTCCATCTGCATTCAT	58	395 bp
Fragment 3	F TGCAGGTTTCTCTACAGTACA R AGACATAACTAATAATGAAGCAG	58	414 bp
Fragment 4	F TGAGTAATAGTGTATTACTCTGT R GAAAAGATTTGGAAGACATCAG	55	494 bp
Fragment 5	F GATTGAAATTCACTTACACCGG R TCTGCAGATAAAAGGCTCTAAG	60	417 bp
Fragment 6	F CTTGAAGATTAGGAGAAACACA R TTAAGGGATTCTCAATATACACA	58	458 bp
Fragment 7	F GCAAGTTATATTAGTGAAGATGG R TCCAAACTACCTATTATGAACTG	60	465 bp
Fragment 8	F TTCTGCAAAGGTGGCAATGC R ATACATATTGTGTCTGTGGTAC	58	365 bp
Fragment 9	F GAGAATTTAAGTAGAAAAGTTGC R TCCAGGTGATATAAGGAGGAC	56	489 bp
Fragment 10	F CTATTTGCTTAAAGTACGCATCTC R TGCATCTGTCGATGACACTGAC	60	534 bp
Fragment 11	F ACTCATCCTGAAAGATAAATGAC R GCTGAATTTTCCTTAGGCTGG	59	515 bp

3.5.3 Cloning and haplotype analysis

After informative polymorphic sites identification, to test in which haplotype (paternal or maternal) MYHRS causative mutations occurred, we proceeded with cloning of fragments encompassing the MYHRS causative mutations and the informative polymorphic site (Table 7). To this purpose, we used Strataclone PCR cloning Kit (STRATAGENE). We transformed provided competent cells using about 50 ng of PCR product, with Strataclone standard protocol. A volume of 150 µl of cells grown in LB medium was plated for each cloning reaction and plates were incubated overnight at 37°**.** 6 colonies were selected and picked from each cloning plate and bacterial inocula were grown over night. After that, bacterial cultures were precipitated by centrifugation and plasmidic DNA was purified with Miniprep Purification Kit (Promega). Sanger sequencing of DNA minipreps and segregation analysis was then performed, in order to evaluate which allele at the polymorphic site was in *cis* with the mutation (Fig. 6).

Table 7. Primer sequences, annealing temperatures and amplicon length for *SMAD4* cloning fragments. Forward or Reverse primer for each amplicon were used to perform Sanger sequencing.

Primers and annealing temperature for *SMAD4* cloning fragments amplification			
SMAD4 cloning fragments	Primer sequence	Tann (°C)	Amplicon length (bp)
Fragment A	F ACTGGGATGATGACATTTTTGA R CATGGTATGAAGTACTTCGTC	60	1551 bp
Fragment B	F TGCAGGTTTCTCTACAGTACA R TAGTTTTCACTCCATGTTTAGC	58	1068 bp
Fragment C	F GATTGAAATTCACTTACACCGG R TAGTTTTCACTCCATGTTTAGC	62	608 bp
Fragment D	F CTATTTGCTTAAAGTACGCATCTC R TGTCTGCTAGGAGCAAGGCAG	64	2481 bp
Fragment E	F GAAAGTATGTACACTTAGCATTC R CATGGTATGAAGTACTTCGTC	56	2573 bp

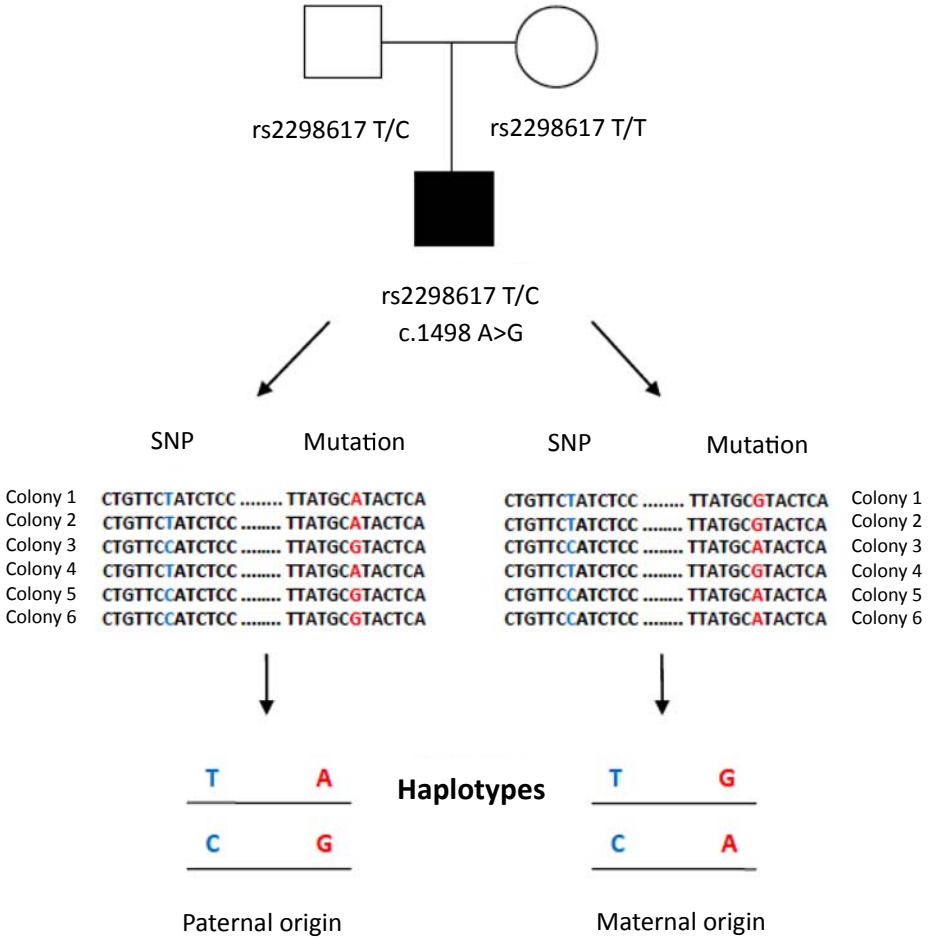

Figure 6. Expected haplotypes from cloning of proband genomic fragment encompassing informative polymorphic change and *SMAD4* mutation. Haplotype is a combination of *in cis* alleles, that are on the same DNA filament. The single nucleotide polymorphism (SNP) here showed has 2 possible alternative alleles (T o C). Proband, heterozygous for the SNP, has inherited C allele from the father (which also is heterozygous for that genomic position) and T allele from the mother (which instead is homozygous). In the same manner, the mutation site, that is heterozygous in the affected case, can show the G allele (mutated) or the A allele (WT). Since the proximity of the SNP to the mutation site, we expect to obtain only 2 haplotypes that will be different because of the paternal or maternal origin of the mutation. In case of paternal origin, we will find G allele (mutated) at mutation site *in cis* with C allele (alternative) at polymorphic site in one haplotype, and A allele (WT) at mutation site *in cis* with T allele (WT) at polymorphic site in the other. Differently, in case of maternal origin, we will find G allele (mutated) at mutation site *in cis* with T allele (WT) at polymorphic site in one haplotype, and A allele (WT) at mutation site *in cis* with C allele (alternative) at polymorphic site in the other. Depending on parental origin, both the expected haplotypes will occur in 50% of the colonies.

4. Results

4.1 Functional characterization of SMAD4 mutants

In order to investigate functional effects of SMAD4 Isoleucine 500 variants causing MYHRS, several distinct cellular assays were performed.

4.1.1 Protein expression analysis

Western blot analysis of cultured skin fibroblasts from cases and passage-matched control, detected enhanced levels of endogenous SMAD4 in MYHRS probands, compared to a weak endogenous level of the protein in the control fibroblasts (Fig. 7a). Furthermore, the transient transfection of HeLa cell line with wild type and mutant SMAD4-Xpress constructs analyzed by immunoblot, showed that MYHRS mutations are sufficient to increase SMAD4 expression levels, suggesting that MYHRS variants affect protein turnover (Fig. 7b), as proposed by Le Goff and coworkers.

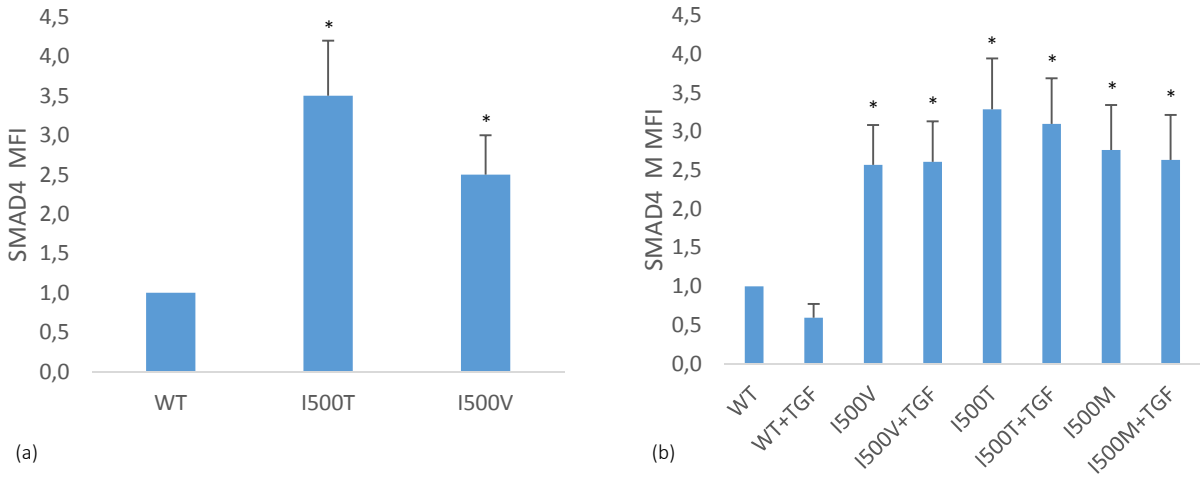

Figure 7. Increased endogenous and ectopic SMAD4 expression in Ile500 MYHRS mutants. (a) Increased SMAD4 expression in MYHRS fibroblasts. Cells were cultured in DMEM High with 10% FBS. WT and MYHRS fibroblasts (cases: TO_01, Ile500Thr mutated and NA_01, Ile500Val mutated) were tested for SMAD4 endogenous level by Western blot analysis. (b) Increased ectopic SMAD4 levels after transient transfection of Ile500 mutants in HeLa cells with and without TGFβ stimuli, with respect to WT transfected cells. SMAD4 content for each sample was normalized to the respective GAPDH content. MFI= Mean Fold Increase. Error bars indicate the standard error of the mean from 3 independent experiments. * p<0.05 compared to WT cells

4.1.2 SMAD4 mutants localization

SMAD4 localization in MYHRS patients fibroblasts has been evaluated through immunofluorescence analysis at confocal laser scanning microscope. MYHRS cells showed enhanced SMAD4 expression, thus confirming Western blot analyses. Moreover, an extra-nuclear accumulation of SMAD4 in MYHRS cases fibroblasts after 2.5 and 5 hours of TGFβ stimulation was observed, contrasting with a lower expression and a prevalent nuclear localization of the protein in control cells (Fig. 8).

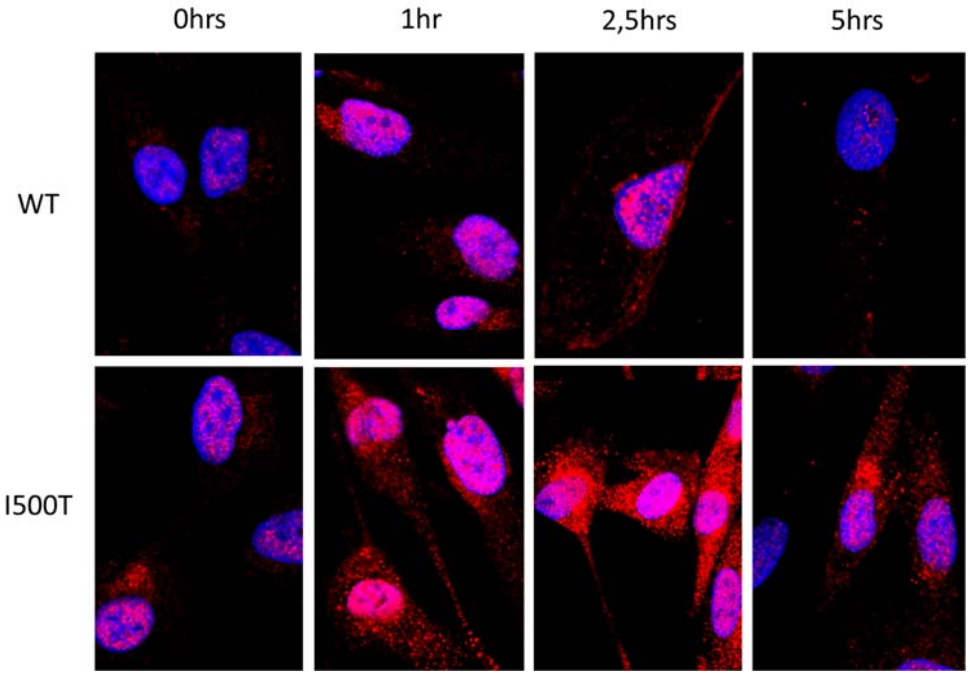

Figure 8. Immunofluorescence analyses by confocal laser scanning microscopy in MYHRS (Ile500Thr) and WT fibroblasts. An evident extra-nuclear accumulation of MYHRS-mutated SMAD4 was detected in patient fibroblasts after 2.5 and 5 hours of TGFβ stimulation. Dapi and anti-rabbit Alexa Fluor®568 secondary antibody were used to detect nuclei and SMAD4 (blue and red respectively).

4.1.3 Proliferation assays

To evaluate the outcome of altered MYHRS-mutated SMAD4 expression and localization, cell proliferation was considered. We firstly performed growth curve analysis on MYHRS patients and control fibroblasts. As shown in Figure 9, MYHRS fibroblasts present a reduction in the proliferation levels compared to control fibroblasts. This difference in growth rate is particularly evident at 6 days of culture, when the amount of control cells is doubled with

respect to MYHRS fibroblasts. Furthermore, BrdU incorporation assay on MYHRS and control fibroblasts as well as on 3T3 WT and MYHRS-mutated SMAD4 transfected cells was carried out. Fluorescence microscopy analysis of BrdU positive cells showed a significantly reduced growth rate ($p < 0.05\%$) in MYHRS patients fibroblasts (Figure 10a). Moreover, we found that overexpression of WT SMAD4 is sufficient to induce proliferation in 3T3 transfected cells, whereas MYHRS-mutated SMAD4 overexpression does not exert any proliferative effect (Figure 10b). These data suggest a loss of function effect of MYHRS-mutated SMAD4.

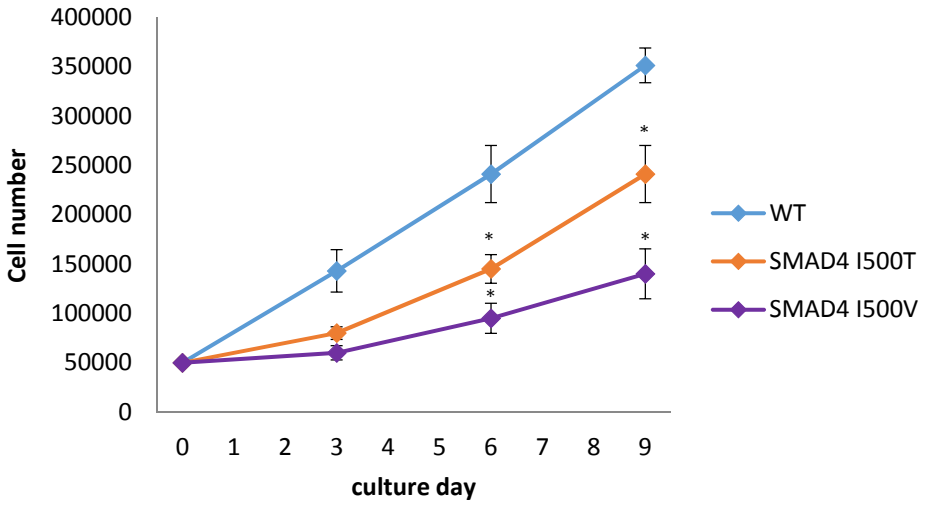

Figure 9. Growth curve of MYHRS-mutated (orange, violet) and WT control (blue) fibroblasts, showing a reduction in the proliferation levels of patient cells compared to WT. Relative cell number versus days are shown. The graph represents the cell number at each time point (triangle, square and diamond for Ile500Val, Ile500Thr and WT fibroblasts respectively). Error bars indicate the standard error of the mean from 3 independent experiments. *P<0.05 in MYHRS-mutated compared to WT cells

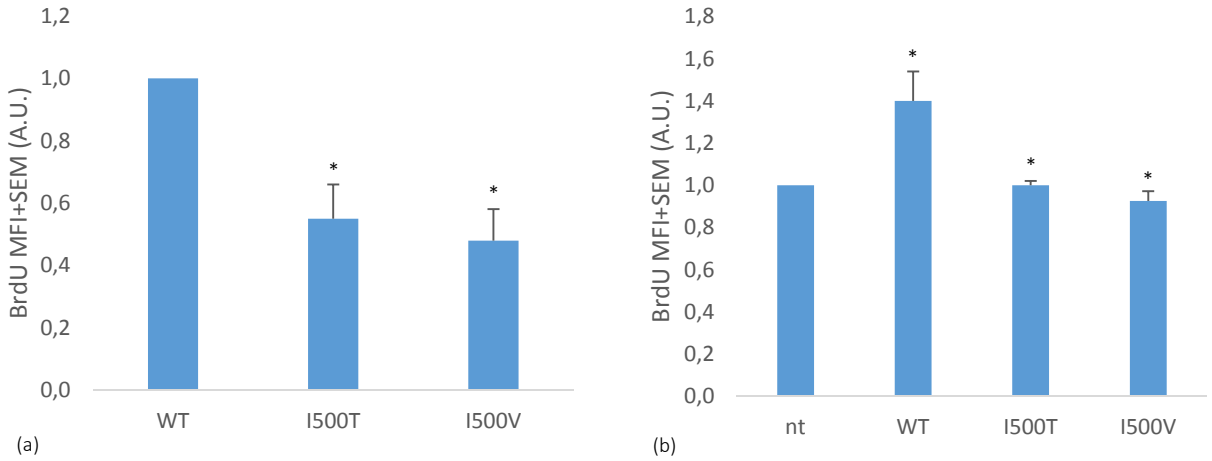

Figure 10. Growth rate of Myhre fibroblasts and transiently transfected cells. (a) BrdU incorporation in MYHRS (TO_01, Ile500Thr mutated and NA_01, Ile500Val mutated) and WT control fibroblasts. After a BrdU pulse of 5 hours, MYHRS affected cells show a reduced proliferation, compared to the WT fibroblasts. (b) Growth rate in 3T3-SMAD4 overexpressing cells. Ectopic expression of MYHRS-mutated SMAD4 is ineffective in inducing cell growth, whereas WT SMAD4 overexpression shows a proliferative effect. Significance were calculated for WT overexpressing cells in respect of not transfected controls, whereas for MYHRS mutants in respect of WT. MFI= Mean Fold Increase. The average and SEM (standard error of measurement) of three independent experiments are shown *P<0.05 in WT compared to nt and in mutants compared to WT

4.2 Molecular screening of *SMAD4* coding sequence

Via molecular screening, we identified *SMAD4* mutations in 4 out of 14 MYHRS collected patients. The previously described *SMAD4* c.1498 A>G mutation (Ile500Val) was found in one patient, whereas a novel mutation in position c.1486 was detected in 3 cases (Table 8). The latter, is a previously unreported mutation that consists of a Cytosine to Thymine transition, which produces an Arginine to Cysteine substitution in position 496 of SMAD4. Parents sequencing for *SMAD4* exon 11 confirmed the *de novo* origin of the 4 mutations and STR genotyping confirmed paternity for these cases. All of 4 probands display typical clinical features of MYHRS syndrome. Electropherograms analysis demonstrated that no mutation affecting *SMAD4* coding sequence was present in the remaining 10 patients.

Exome Sequencing (WES) approach was applied to a selection of *SMAD4* mutation negative patients: data analysis is still in progress.

Table 8. Nucleotide change and amino acid substitution for *de novo* mutations affecting *SMAD4* identified in our MYHRS cohort by molecular screening.

Case	Nucleotide change	Aminoacid substitution	Inheritance	Provenance
GM13-0400	c.1486 C>T	Arg496Cys	*De novo*	San Camillo-Forlanini Hospital
RM_01	c.1498 A>G	Ile500Val	*De novo*	Fatebenefratelli Hospital
TO_04	c.1486 C>T	Arg496Cys	*De novo*	Torino University
TO_05	c.1486 C>T	Arg496Cys	*De novo*	Torino University

4.3 Novel *SMAD4* mutation

For one out of the 3 MYHRS patients with *SMAD4* mutation c.1486 C>T (Arg496Cys), we also collected samples of hair bulb and buccal mucosal epithelial cells. Genomic DNA extraction from these additional tissues (performed with standard protocol), amplification and sequencing of the relevant exon provided evidence for the germline origin of the mutation (Fig. 11). Arginine in position 496 of SMAD4 is conserved among orthologs (Figure 12) and a conservative missense change affecting this residue, p.Arg496His, had previously been reported as somatically acquired lesions in human cancers (Lazzereschi *et al.*, 2005; Fleming *et al.*, 2013). All of 3 patients display typical MYHRS clinical characteristics, such as muscular build, joint stiffness, brachydactyly of hands and feet and recognizable facial dysmorphisms.

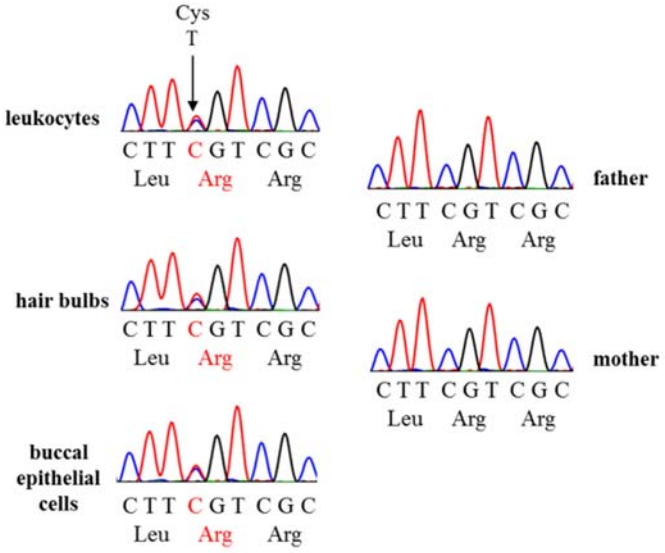

Figure 11. Electropherograms showing the *de novo* germline origin of the c.1486C>T transition in *SMAD4* (patient GM13-0400, from Caputo *et al.*, 2014).

The missense change (p.Arg496Cys) was identified at the heterozygous state in all patient's tissues (circulating leukocytes, buccal mucosal and hair bulb epithelial cells), documenting its germline origin.

Figure 12. Amino acid sequence alignment of the MH2 domain portions of SMAD4 orthologs. Conserved Arg496 amino acid is indicated by the black arrow (from Caputo *et al.*, 2014).

4.3.1 Structural analysis

To prove the causal involvement of this novel mutation in the occurrence of the clinical phenotype, *in silico* structural analysis were performed in collaboration with Prof. Gianfranco Bocchinfuso and Prof. Lorenzo Stella of Tor Vergata University. Previous works reported the impact of the disease-causing amino acid changes affecting Ile500 on SMAD4 binding to other SMAD proteins and on ubiquitination, which is known to control SMAD4 degradation via proteasome (Caputo *et al.*, 2012; Le Goff *et al.*, 2011a). Structural analyses explored the consequences of the novel MYHRS-causing mutation on SMAD4 function. Arg496 is located in the MH2 domain (Fig. 13a), which mediates SMAD4 binding to activated receptor-regulated SMAD proteins (R-SMADs), and formation of the functionally active heterotrimer complex (Chacko *et al.*, 2001; Wu *et al.*, 2001; Kuang and Chen, 2004; Bourgeois *et al.*, 2013). The MH2 domain contains two subdomains, the three-helix bundle extension and the β-sandwich core. This domain is involved in R-SMAD binding through two different interfaces (interface 1 and interface 2) (Fig. 13a). Residue Arg496 is located within the three-helix bundle at interface 1 and is specific for SMAD4 proteins, being substituted by a neutral residue in paralogs. To investigate the role of Arg496 in trimer stability, we identified the R-SMADs interacting residues. The sequence homology between the MH2 domain of SMAD3 and those of SMAD1,

SMAD5, and SMAD9 is about 80%. In all proteins, a highly conserved motif comprising four invariant residues (i.e., Gly272, Ser275, Asn276 and Arg279, in SMAD3) was identified. Arg496 was not observed to form any specific interaction (salt bridges or strong H-bonds) with these residues, questioning its direct contribution to the complex stability. Arg496 interacts with Ile500 which is located close to the protein surface, is solvent accessible for only 6% of the residue surface, and interacts with the hydrocarbon part of the side chains of residues Arg497, Arg502, Glu526, and His528. These residues constitute a basic pocket with a characteristic structural topology and very peculiar electrostatic features. Of note, this pocket is placed close to Lys519, which is one of two ubiquitination sites in SMAD4 (Fig. 13b). Searching for available structures possessing a group of residues in a topology similar to this motif identified three structures with a root mean square displacement of their Cα and Cβ atoms lower than 1.0A with respect to the reference motif (pdb codes: 1n3g, RMSD 0.63A; 1h8c RMSD 0.71A; 1ghp, RMSD 0.93A). Among them, 1h8c corresponds to the structure of an UBX domain, where the motif residues corresponding to those of SMAD4 are Lys46, Arg53, Arg54, Glu79, and Phe77 (Fig. 13c). The conformation of this domain is almost superimposable with the structure of the ubiquitin domain dimer (pdb code 1aar), which contains a basic pocket similar to that investigated here (Cook *et al.*, 1992; Buchberger *et al.*, 2001). In particular, the 1aar structure residues Arg74, Arg72, Arg42, and Asp39 are located close to the interface between the two ubiquitin domains, and undergo a conformation rearrangement during dimerization (Cook *et al.*, 1992). This structural similarity suggests a role of this motif in the priming interaction with ubiquitin required for ubiquitination of Lys519 (Caputo *et al.*, 2014).

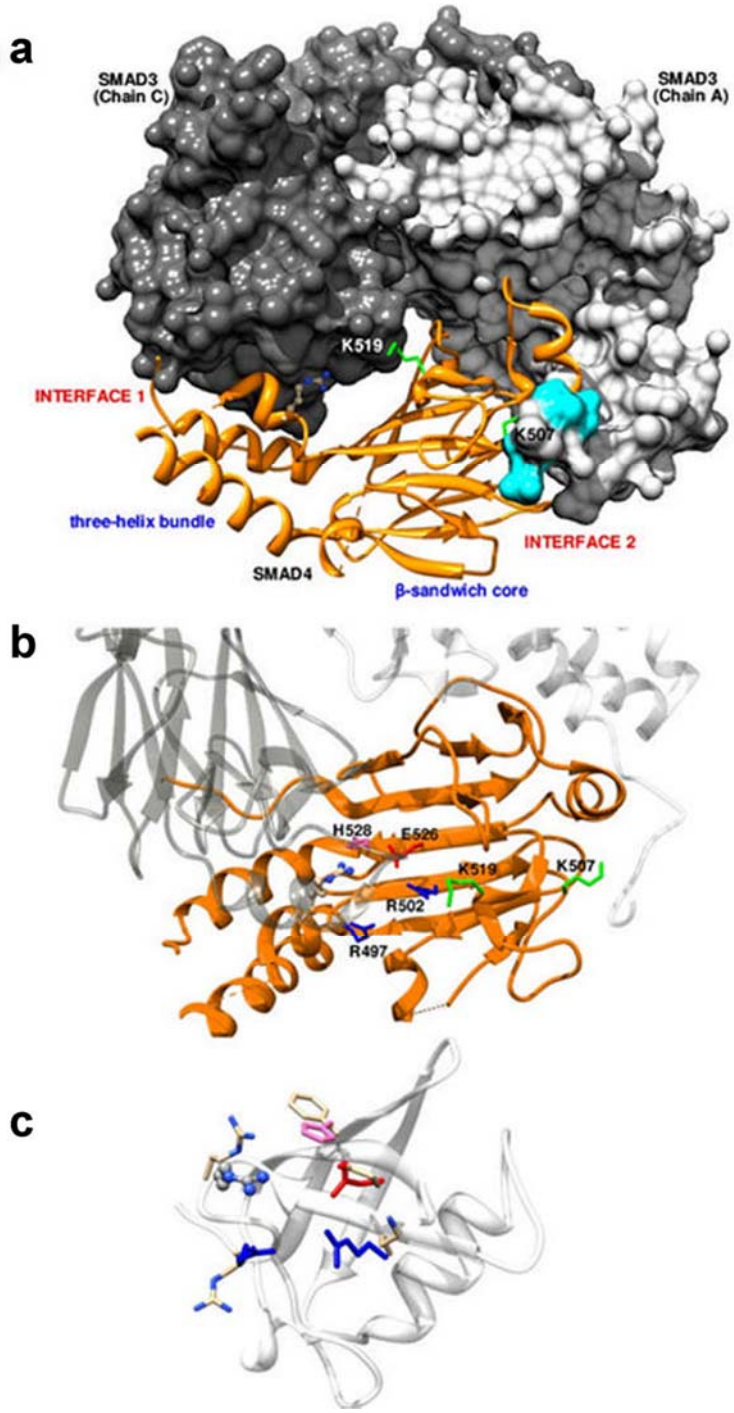

Figure 13. Structural analyses exploring the consequences of the novel MYHRS-causing mutation on SMAD4 function (from Caputo *et al.*, 2014).

(a): Location of Arg496 in the structure of the SMAD3/SMAD4 MH2 domain complex (pdb code 1u7f). The SMAD4 chain is represented as an orange ribbon, the heavy atoms of the Arg496 side chain are depicted as ball and stick (C in brown and N in blue). The two sites of ubiquitination in SMAD4 (Lys519 and Lys507) are reported as green sticks. The SMAD3 MH2 domains are reported as surfaces. The two chains reported in the pdb file are colored in dark (chain C) and light (chain A) gray. In SMAD3, chain A, the serine residues that are subjected to phosphorylation are colored in cyan.

(b): Region surrounding Arg496 in the SMAD4 MH-2 domain. Coordinates are taken from the structure of the SMAD4 and SMAD3 MH-2 domains complex (pdb code 1u7f). SMAD4 and Arg496 are reported as in (a), SMAD3 chains are shown as semi-transparent light gray (chain A) and dark gray (chain C) ribbon. Other residues are also evidenced as sticks. The other arginine residues belonging to the basic pocket discussed in the text are colored in blue (Arg497 and Arg502), Glu526 is colored in red and His528 in pink. The ubiquitination sites in SMAD4 (Lys519 and Lys507) are

colored in green. c: Structure of the UBX domain (pdb code 1h8c). Residues Arg53, Arg54, Lys46, Glu79, and Phe77, matching the structural motif in SMAD4, are reported as sticks (N is colored in blue, O in red, and C in brown). For comparison, the residues constituting the structural motif in SMAD4 (Arg496, Arg497, Arg502, Glu526, and His528) are also reported with the same convention used in (b).

4.3.2 Methylation analysis

4.3.2.1 The c.1486 C>T transition localizes in a methylated CpG dinucleotide

We preliminarily investigated methylation as a potential driving force for the occurrence of p.Arg496Cys variation, since the triplet coding for the Arginine at position 496 encompasses a CpG dinucleotide. DNA amplification success after Hpy99I methylation-sensitive endonuclease digestion, confirmed that cytosine at position c.1486 is methylated (Fig. 14). This finding is in line with annotations of several methylation databases (Fig. 15). The complete digestion of a PCR amplified fragment (WT amplicon in Fig. 14) proved the ability of the restriction enzyme to cut unmethylated DNA at the recognition sequence.

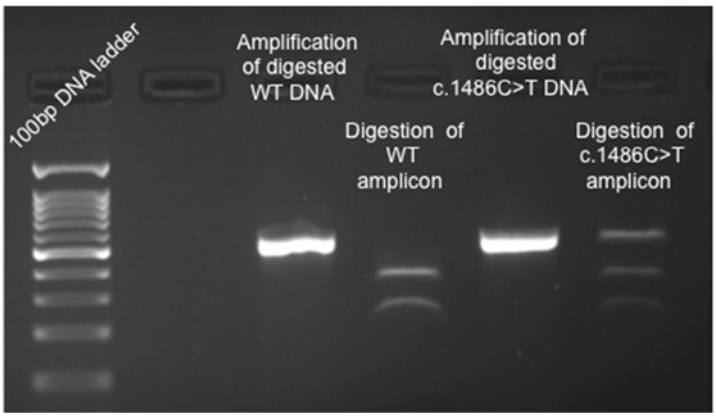

Figure 14. 2% agarose gel showing WT and c.1486 C>T heterozygous genomic DNA/PCR product digestion with Hpy99I methylation-sensitive restriction enzyme. Gel electrophoresis was performed for 30 minute at 80 mV.

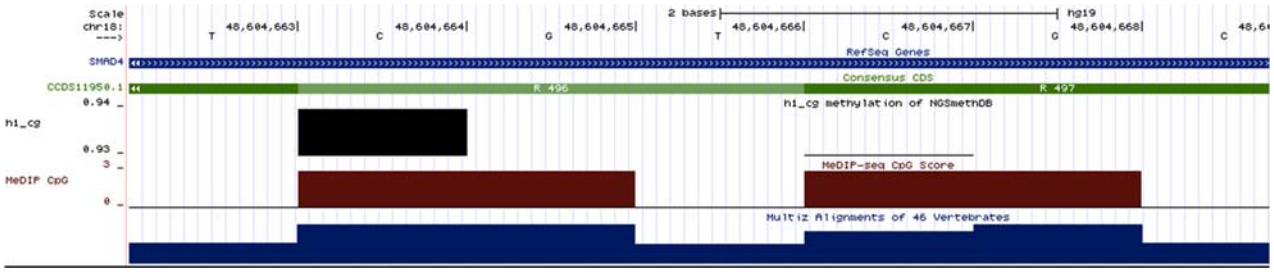

Figure 15. Methylation status of *SMAD4* CpG dinucleotides at 496 and 497 codons, as reported in MeDIP CpG and NGSmethDB (annotations are visualized through UCSC Genome Browser, GRCh37/hg19 Assembly); https://genome.ucsc.edu/.

4.3.2.2 *SMAD4* mutations encompassing CpG sites in *SMAD4* coding sequence

Sistematic *in silico* analysis of mutations localized in *SMAD4* CDS, performed using several human mutation databases, suggested that methylation could be the mechanism responsible for several pathogenic germline and somatic mutations in this gene.

All 28 *SMAD4* coding CpGs were reported as methylated in 1 or both methylation databases that have been interrogated.

We observed that 21 out of 28 *SMAD4* coding CpG dinucleotides harbor transitions, reported in Exac and dbSNP databases (26 annotated nucleotide changes) as polymorphisms.

Moreover, from OMIM, ClinVar and HGMD databases, we found that 9 *SMAD4* coding CpGs are affected by mutations (12 transitions reported) known to cause genetic disorders, Juvenile polyposis syndrome (MIM 174900), Juvenile polyposis with hereditary hemorrhagic telangiectasia (MIM 175050) and Hereditary cancer-predisposing syndrome (MedGen UID 14326). Further, 27 somatic transitions reported in COSMIC as cancer associated, localize in 20 out of 28 *SMAD4* CpG dinucleotides.

4.4 Parental origin of mutations

4.4.1 Informative polymorphic sites research

DNA amplification and sequencing of genomic fragments near causative MYHRS mutations in 16 MYHRS *SMAD4* positive probands made possible the identification of 13 heterozygous polymorphic sites. Segregation analysis in parents, confirmed the presence of 11 informative SNP in 11 affected cases. We identified 4 families informative for polymorphism rs2298617 T/C, 3 families informative for rs72913266 C/G, 1 family informative for rs11663403 C/T, 1 family informative for rs2298617 T/C, 1 family informative for rs114637817 and 1 family informative for an unreported intronic change c.11447+610 T/delT. Genotypes of other 11 analyzed high frequency polymorphisms turned out to be WT homozygous in the probands.

4.4.2 Cloning and haplotype analysis

Subcloning of genomic fragments encompassing MYHRS causative variant and informative polymorphic site allowed the determination of haplotypes in 11 probands. Electropherograms analysis showed that bacterial colonies, harboring single stranded DNA of each proband, presented both possible haplotypes with a frequency of about 50%. Sequencing and segregation analysis demonstrated the paternal germline origin of the mutations in all informative cases (Fig. 16, Table 9).

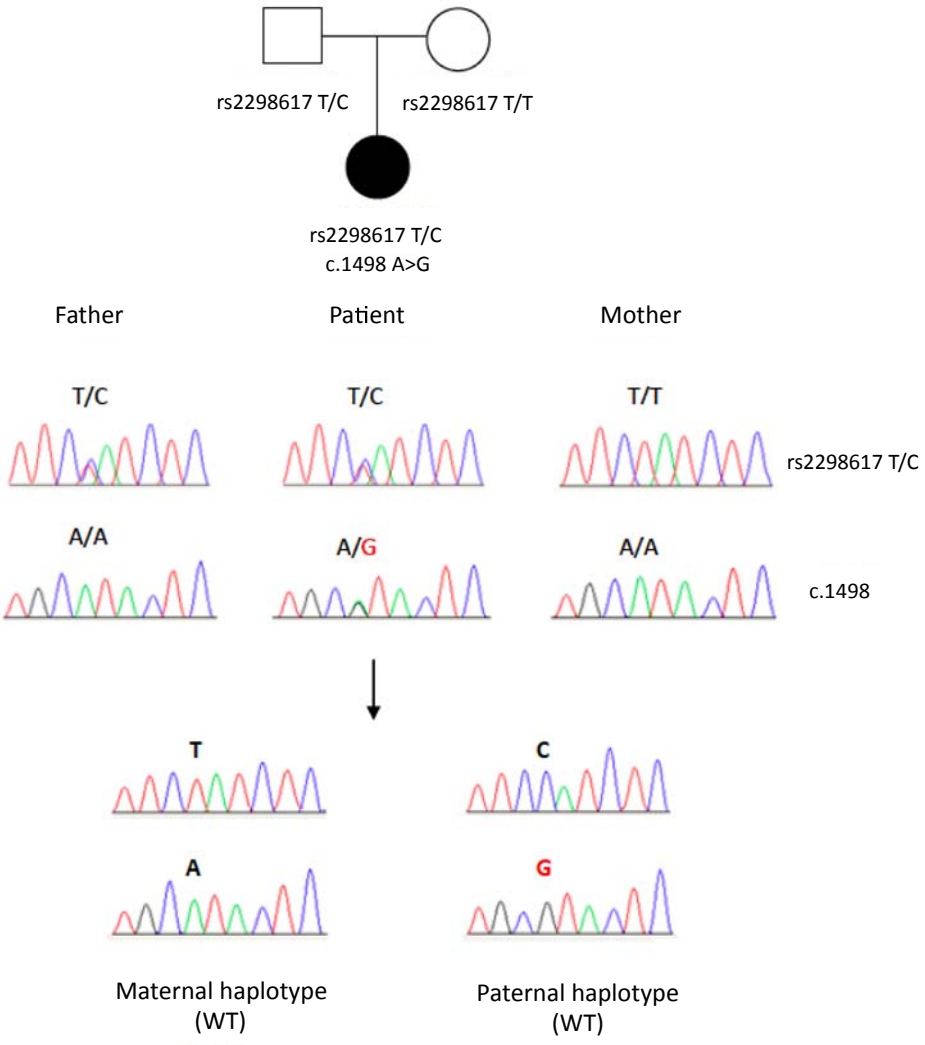

Figure 16. Results obtained from Sanger sequencing of TO_03 proband family. The patient and her father are heterozygous (T/C genotype) for rs2298617, which flanks the MYHRS causative mutation (c.1498A>G). The patient is heterozygous at the mutation site too (affected), whereas the two parents are WT (unaffected subjects). Haplotypes were determined by amplification and cloning of proband genomic DNA fragment containing the polymorphic and

MYHRS mutation sites. Parental genotypes at the intronic polymorphic and mutation sites were determined by amplification and direct Sanger sequencing.

Table 9. Parental origin of *de novo SMAD4* mutations causing MYHRS

Case	Mutation	SNP	SNP Genotype			Haplotype	Origin
			Father	Mother	Case		
TO_03	c.1498A>G	rs2298617 T>C	T/C	T/T	T/C	1498G, rs2298617C	paternal
NA_01	c.1498A>G	rs2298617 T>C	T/T	C/C	T/C	1498G, rs2298617T	paternal
NA_02	c.1498A>G	rs2298617T>C	C/C	T/T	T/C	1498G, rs2298617C	paternal
TO_01	c.1499T>C	c.1447+610 T>delT	T/T	T/delT	T/delT	1499C, 1447+610T	paternal
CA_01	c.1499T>C	rs11663402 C>T	C/C	C/T	C/T	1499C, rs11663402C	paternal
GM-13-0400	c.1486 C>T	rs2298617 T>C	T/C	T/T	T/C	1486T, rs2298617C	paternal
TO_02	c.1498A>G	rs543260206 G>A	G/A	G/G	G/A	rs543260206A, 1498G	paternal
2P	c.1499T>C	rs72913266 C>G	C/C	C/G	C/G	rs72913266C, 1499C	paternal
4P	c.1499T>C	rs114637817 A>T	A/T	A/A	A/T	1499C, rs114637817T	paternal
RE_01	c.1499T>C	rs72913266 C>G	C/G	C/C	C/G	rs72913266G, 1499C	paternal
TO_04	c.1486 C>T	rs72913266 C>G	C/C	C/G	C/G	rs72913266C, 1486T	paternal

5. Discussion

Myhre syndrome (MYHRS) is a rare developmental disorder characterized by cognitive deficit, facial dysmorphisms, deafness, stiff joints and distinctive musculoskeletal features. Based on several MYHRS representative clinical findings, such as muscular build (97% of cases), joint limitation (81-84% of patients), from 2SD to 5.5SD postnatal growth retardation (68,7% of cases) and the presence of small hands and feet (96.8% of probands), this syndrome was ascribed to the acromelic dysplasia group, which to date includes other three disorders displaying a partially overlapping phenotype, namely Weill-Marchesani syndrome, geleophysic dysplasia and acromicric dysplasia. Although partially similar, these four conditions can be distinguished by virtue of subtle clinical features as well as by their pattern of inheritance (Le Goff and Cormier-Daire, 2012). The identification of the acromelic dysplasias molecular bases allowed to disclose the common pathogenic mechanism underlying these disorders, such as the alterations of the transforming growth factor β (TGFβ) signaling. This pleiotropic cytokine signaling network plays an important role from early embryogenesis to adulthood. It controls different cellular processes, including cell division, differentiation, migration, adhesion, organization and programmed cell death through the action of TGFβ and its family members, such as the nodals, activins, bone morphogenetic proteins (BMPs), myostatin and anti-Muellerian hormone (AMH) (Massagué and Gomis, 2006). In this pathway, SMAD4 acts as a common partner of activated R-Smads to help execute their function of target gene transcription regulation. Moreover, SMAD4 has been established as a tumor suppressor, since loss-of-function mutations in this gene are known to cause two familiar cancer-prone diseases (juvenile polyposis syndrome (JPS, MIM 174900) and Juvenile polyposis/hereditary hemorrhagic telangiectasia (JPHT, MIM 175050)) and occur in different types of carcinomas, such as pancreas, gastrointestinal tract and skin.

In this work, we performed different cellular assays, in order to characterize expression and localization of MYHRS-mutated SMAD4 and cell proliferation in affected fibroblasts as well as in transiently transfected cell lines.

Our data on MYHRS Ile500Val and Ile500Thr mutants in primary fibroblasts and overexpressing cells lines show a significantly increased SMAD4 expression, confirming data obtained by Le Goff and collaborators, as well as by Piccolo and colleagues on MYHRS primary fibroblasts carrying Ile500Thr, Ile500Val and Arg496Cys substitutions, respectively. Since SMAD4 is monoubiquitinated at Lysine in position 519, which is located close to Ile500 in the

three-dimensional structure of the protein, the elevated SMAD4 level in MYHRS–cells can be explained as the consequence of impaired SMAD4 ubiquitination, resulting in increased stabilization of the mutated protein. This hypothesis is supported by the decresead SMAD4 ubiquitination levels shown by Le Goff and collaborators in a single case of MYHRS-affected fibroblasts. Furthermore, the possible impairment of the SMAD4 ubiquitination as a consequence of Ile500 MYHRS-mutations is in line with the previously published structural models of SMAD4 Ile500 mutants (Caputo *et al.*, 2012, Le Goff *et al.*, 2011a), which suggested that amino acid substitution causing Myhre syndrome might affect proper SMAD4 ubiquitination, perturbing the signal flow by increasing the intracellular concentration of non-ubiquitinylated SMAD4 (Caputo *et al.*, 2012). Moreover, our observation that mutant SMAD4 accumulates outside the nucleus (Fig. 8) strengthens the hypothesis of an altered SMAD4 degradation in Myhre cells.

Preliminary experiments indicate that cytoplasmic accumulated SMAD4 mostly colocalizes with RAB11 in affected fibroblasts (data not shown). This is a ubiquitously expressed protein associated with recycling endosomes, which function in the delivery of proteins destined for trans-Golgi network and plasma membrane. These preliminary evidences suggest that SMAD4 might localize aberrantly during TGFβ response in Myhre fibroblasts, possibly interacting with other cellular or extracellular matrix structures.

SMAD4 molecular screening performed on a selected cohort of Myhre-like patients, detected 4 *de novo* mutations in *SMAD4* coding sequence, 3 of which consist of a previously undescribed mutation (c.1486 C>T) affecting Arg496 residue of SMAD4.

Our SMAD4 p.Arg496Cys structural model shows that Arginine in position 496 interacts with Ile500 residue. The latter, in turn interacts with four residues constituting a basic pocket placed close to the ubiquitination site Lys519, thus suggesting that also p.Arg496Cys substitution might perturb the regulatory mechanism controlling SMAD4 ubiquitination.

Consistently, Piccolo and collaborators showed increased SMAD4 protein levels, although with a lesser extent than Ile500 mutants, in MYHRS cells harboring the Arg496Cys substitution, therefore supporting a possible role of this variant in SMAD4 impaired ubiquitination.

Furthermore, the present structural analysis excludes a major contribution of the Arg496 amino acid change to the complex stability. In agree with this, previous studies documented that the p.Arg496Ser change does not prevent heterotrimer formation, although it was found

to partially impair the transcriptional activity of the complex itself (Chacko *et al.*, 2001). On the one hand structural and expression level analyses of the mutant protein as well as clinical features of our 3 SMAD4 p.Arg496Cys patients support the overall functional equivalence of c.1486 C>T transition to MYHRS causative missense mutations affecting Ile500. On the other hand, the evidence that cancer-associated missense mutations affect residues mutated in MYHRS (i.e. p.Arg496His, c.1487 G>A. Lazzereschi *et al.*, 2005; Fleming *et al.*, 2013) or spatially close codons (Asp493 , Asp494 , Leu495 , Cys499 , Arg502 , Ser504 , Phe505 , and Val506) (COSMIC database, http://cancer.sanger.ac.uk/cancergenome/ projects/cosmic/) highlights the dramatically diverse impact of apparently subtle perturbation of SMAD4 structure and function on intracellular signaling and gene expression. Therefore, it is possible that different MYHRS mutations, although resulting in the same clinical phenotype, may exert different effects on TGFβ and BMP target genes expression, possibly producing subtle changes in clinical manifestations that have not been clearly noticed so far. Consistently with this hypothesis, a different matrix metalloproteinases and related inhibitors gene expression pattern was detected by Piccolo and colleagues in MYHRS fibroblasts harboring the SMAD4 p.Ile500Val with respect to p.Arg496Cys substitution. In particular, MYHRS fibroblasts bearing the p.Ile500Val substitution showed increased expression of MMP2 and MMP14 and downregulation of their inhibitors SERPINE1 and TIMP3 compared to healthy controls, whereas affected MYHRS p.Arg496Cys cells presented a significant increase in metalloproteinases, but no decrease in SERPINE1 and TIMP3 expression levels (Piccolo *et al.*, 2014). Moreover, although the small number of reported MYHRS patients harboring c.1486 C>T mutation (p.Arg496Cys) (McGowan *et al.*, 2011; Michot *et al.*, 2014, and our 3 patients) does not allow a statistically significant genotype-phenotype correlation, it has been noted that Arg496 patients show neither short stature nor heart malformation, nor cardiac long term complications (Starr *et al.*, 2015). Therefore, analyses of the expression of other SMAD4-complex target genes in MYHRS Ile500 and Arg496 mutant cells are requested in order to shed light on possible different impacts of MYHRS mutations in gene transcription and downstream signaling pathways.

Since TGFβ signaling is known to activate proliferation and to induce apoptosis resistance in fibroblasts (Gardner *et al.*, 2004), we decided to investigate possible alteration of this process in MYHRS cells. Here, we detect a decreased cell proliferation of MYHRS fibroblasts, with respect to matched control cells. Moreover, overexpression of Ile500 MYHRS mutants failed in inducing cell proliferation, whereas WT overexpression increases growth rate of transfected

cells. Our data support a loss of function effect on proliferation for MYHRS p.Ile500 mutations. Consistent with this, Piccolo and collaborators identified a reduction in expression levels for *SERPINE1* and TIMP3 TGFβ target genes in SMAD4 Ile500-mutated fibroblasts. Moreover, MYHRS fibroblasts have been showed to exhibit impaired microfibrillar deposition, displaying a statistically significant reduction of FBN1 staining (Piccolo *et al.*, 2014).

However, mutated-SMAD4 intracellular accumulation and further data on matrix metalloproteinases gene expression (Piccolo *et al.*, 2014), suggest that SMAD4 MYHRS mutations may also exert positive role on TGFβ signaling. In particular, MYHRS mutations have been reported to cause the constitutional activation of TGFβ pathway. This phenomenon was observed in patients fibroblasts, which showed increased phosphorylated SMAD2 (pSMAD2)/total SMAD2 ratio compared with unaffected controls (Piccolo *et al.*, 2014).

Increased signaling and defective extracellular matrix (ECM) deposition are characteristics shared by other acromelic dysplasias, such as acromicric dysplasia and geleophysic dysplasia (Le Goff and Cormier-Daire, 2012), suggesting these features as the common functional outcome of different mutations causing partially overlapping disorders. Although, on the one hand, these findings link the increased TGFβ signaling and impaired matrix deposition to short stature phenotypes, on the other hand a similarly enhanced TGFβ signaling and microfibrillar changes were detected also in Marfan syndrome (MIM 154700), which display an opposite skeletal phenotype, with long bone overgrowth and arachnodactyly. If this issue emphasizes the importance of a carefully controlled TGFβ signaling in skeletal biology, nevertheless, how the activation of this pathway can results in clinically opposing effects needs further investigations.

As it is well known, TGFβ is the predominant cytokine in all forms of fibrotic reactions, and is implicated in pulmonary fibrotic disorders such as idiopathic pulmonary fibrosis (Khalil *et al.*, 2005). Moreover, Gramley and collaborators demonstrated that SMAD4 has increased expression in patients with cardiac atrial fibrosis (Gramley *et al.*, 2010).

In addition, mouse models proved the direct involvement of SMAD4 in cardiac tissue fibrosis. A mouse model with cardiac myocyte-specific disrupted SMAD4 developed heart failure secondary to significant cardiomyocyte hypertrophy and cardiac fibrosis (Wang *et al.*, 2005). Furthermore, cardiac tissue fibrosis has also been induced in cardiac fibroblasts from a mouse model directly targeting SMAD4, increasing the profibrogenic TGFβ1 activity (Huang *et al.*, 2014).

Recently, Starr and co-workers reported on 5 patients with Ile500 substitutions, which had significant cardiac and/or pulmonary pathology and abnormal wound healing. Among them, 2 probands underwent to cardiac transplantation and died for post-surgical complications, principally due to a progressive and markedly abnormal fibroproliferative response to surgical intervention. The apparent contrast between these findings and our proliferation data, while confirming possible dual role of *SMAD4* mutations in TGFβ signaling, suggest that short term *in vitro* experiments might not disclose long term effects of Myhre variants on TGFβ signaling, which are instead likely to occur *in vivo.* Long term *in vitro* experiments may thus help to elucidate other compensative mechanisms triggered by the mutants on TGFβ signaling.

Here, we prove that Myhre mutations c.1498 A>G (p.Ile500Val), c.1499 T>C (p.Ile500Thr) and c.1486 C>T (p.Arg496Cys) have paternal origin in all 11 tested MYHRS cases. This finding confirms previous studies on several conditions, supporting a predominance of paternal origin of point mutations in the majority of autosomal dominant disorders. Studies on diseases arising from lesions affecting fibroblast growth factor receptor (FGFR) gene family, such as Apert syndrome, Achondroplasia, Crouzon syndrome, Pfeiffer syndrome and Muenke syndrome, have demonstrated the paternal origin of these disorders (Moloney *et al.*, 1996; Wilkin *et al.*, 1998; Glaser *et al.*, 2000; Rannan-Eliya *et al.*, 2004). Among others, complete or high prevalence of paternally derived gene mutations have also been documented in type I neurofibromatosis (Jadayel *et al.*, 1990), multiple endocrine neoplasia 2A and 2B (Schuffenecker *et al.*, 1997; Carlson *et al.*, 1994), retinoblastoma (Kato *et al.*, 1994), Noonan syndrome (Tartaglia *et al.*, 2004), Costello syndrome (Sol-Church *et al.*, 2006) and in the X-linked condition Rett syndrome (Trappe *et al.*, 2001). Almost all of these disorders are associated with advanced paternal age, which is known to increases the risk of new germline mutations (Snajderova *et al.*, 2012). Indeed, since the high number of cell divisions that occur in spermatogonial stem cells during male reproductive life, the male germ line of older men is expected to accumulate point mutations principally due to replication errors. Furthermore, reduced activity of repair enzymes, strand mispairing of short tandem repeats and longer exposure to environmental mutagens are also considered as an increasing source of point mutations, as men age (Thomas, 1996; Crow, 2000). Moreover, advanced paternal age affects testicular function, reproductive hormones, sperm parameters, sperm DNA integrity, telomere length, chromosomal structure and epigenetic factors. In this way, it impairs also fertility and reproductive outcomes in older couples, contributing to higher incidences of

congenital birth defects and fetal deaths. Even if advanced paternal age is clearly linked to a higher mutation rate in man germline as well as to other factors which impair fertility, however, medical literature is lacking of an accepted threshold which defines the advanced paternal age. While an age of a father at time of conception of ≥ 40 is considered as a threshold for advanced paternal age more than any other age (Friedman, 1981; de la Rochebrochard *et al*., 2003; Toriello and Meck, 2008), still there is not a unanimous agreement in this category of studies as well as in medical counseling. Recently, several whole-genome (WGS) and whole-exome sequencing (WES) studies have directly observed sequence data to confirm the effect of paternal age (Wong *et al.*, 2016). Kong and colleagues, sequenced the entire genomes of 78 Icelandic parent–offspring trios, and reported a large linear paternal age effect, which consists of more than 2 extra mutations per year in the male germline, and an estimated exponential effect of paternal mutations doubling every 16.5 years. Another study, performing WGS of three multi-sibling families, determined that the number of *de novo* mutations increase with father's age by 2.87 mutations per year, but also detected subtle differences between families (Rahabari *et al.*, 2016). Both studies linked mutation rate in a population to father's age, stating that the major factor influencing the number of mutations in a child is paternal age.

As regards Myhre syndrome, Michot and colleagues reported a high average paternal age at birth for MYHRS patients (> 36 years). This hypothesis was also suggested before *SMAD4* discovery as the molecular cause of the syndrome, since the advanced paternal age of several MYHRS cases (Davalos *et al.*, 2003). Although it is difficult for us to discuss advanced paternal age with a statistical approach, since the small number of cases and their different nationalities, analysis of father ages of our MYHRS cohort do not reveal a significantly higher average paternal age (33.9) in respect to control population. Nevertheless, since the high paternal age reported for many MYHRS affected cases, it is reasonable to think that advanced paternal age can play a role in MYHRS mutations occurrence. Moreover, since the exclusive paternal origin of our cohort, it is probable that other mechanisms contribute to the paternal origin of MYHRS variants. The term ''paternal age effect'' (PAE) disorders, indicates a small group of conditions, including Apert syndrome (caused by FGFR2 mutations), achondroplasia (FGFR3), Noonan syndrome (PTPN11), and Costello syndrome (HRAS), for which molecular basis of this effect has been explained by a mechanism, termed ''selfish spermatogonial selection''. This mechanism, which likely occurs in all men, combining hypermutability of specific nucleotides, expression of this mutant in spermatogonial stem cells and further

positive selection resulting in localized clonal expansion, has been demonstrated, among others, for recurrent mutations of FGFR2 and FGFR3 in Apert syndrome and achondroplasia (Goriely and Wilkie, 2012). Syndromes belonging to the small PAE class share a triad of unusual charateristics: an extreme bias in paternal origin of mutations (α>20), a strong paternal age effect (fathers are on average more than 2 years older than the matched general population), and a high apparent germline mutation rate (>10^{-6}). Also if Myhre syndrome does not strictly satisfies this criteria, the absence of maternal germline derived mutations let us think that Myhre syndrome share at least some characteristics with this class of conditions. As regards MYHRS, a paternal age effect, combined with the prevalence of Ile500 substitution due to mainly two nucleotides changes in *SMAD4*, may suggest a mechanism of protein-driven selfish selection in sperm, as noted by Michot and colleagues. Interestingly, a seminoma testicular germ cell tumors analysis revealed a *SMAD4* 1-bp insertional mutation producing a truncated protein at codon 492, which potentially abrogates TGFβ anti-proliferative effect in stem germ cells (Bouras *et al.*, 2000). Further studies on mutation detection in sperm of fathers and on spatial distribution of the mutation in whole testis will be needed to test the selfish spermatogonial selection hypothesis in Myhre cases (Michot *et al.*, 2014).

A section on spontaneous mutations that show bias with respect to their parental origin is present in the imprinted gene and parent-of-origin effect database (www.otago.ac.nz/IGC, Glaser *et al.*, 2006). To date, a relatively high number of distinct point mutations with paternal origin, causing several autosomal dominant disorders, are reported in the database and a significant portion of those arise in CpG dinucleotides. These sites are known to be mutational hotspots in mammals, ostensibly because spontaneous oxidative deamination of methylated cytosines leads to an increase in transition mutations (Coulondre *et al.*, 1978). Recently, the observed rate of transitions at CpG dinucleotides was estimated as 18.2 times that at non-CpG sites (Kong *et al.*, 2012). Here, we describe a new Myhre transition mutation, which localizes in a CpG dinucleotide. Performed restriction analyses, seem to confirm the methylation status of the involved cytosine, as reported in several methylation databases. In the next future, we have planned to carry out DNA bisulfite modification experiments, in order to further support our findings on methylation status of the c.1486 C nucleotide. DNA methylation is an important epigenetic marker associated with gene expression regulation in eukaryotes. While promoter methylation is relatively well characterized, and is strongly associated with gene silencing, the role of intragenic DNA methylation is still unclear (Singer *et al.*, 2015) and has been mostly shown to associate with transcription elongation (Lister *et al.*, 2009; Aran *et al.*,

2011; Varley *et al.*, 2013). Although it has been documented that exclusive paternal origin can occur without any substitution at CpG dinucleotides in autosomal dominant disorders, still DNA methylation is a major contributor to point mutations leading to human genetic disease, as indicated by germline lesions within a CpG site recurring among patients affected by achondroplasia, Li–Fraumeni syndrome and hemophilia (Martinelli *et al.*, 2008). Interestingly, considering *de novo* germline mutations at CpG and non-CpG sites, Kong and collaborators demonstrated that, as a man ages, rates of all point mutation types increase by a similar factor, not changing the ratio between the different classes. Moreover, the higher level of DNA methylation in spermatogonia, compared with that in oogonia, has been suggested as an important contributing factor in the gender-bias of point mutations, since the greater number of paternally derived point mutations occurs within a CpG dinucleotide. This was bolstered by studies of Apert syndrome, for which the FGFR2 mutation that affects a CpG dinucleotide is twice as prevalent as the one that does not (Moloney *et al.*, 1996). To test whether methylation status in germ line has a detectable impact on mutations, Rahabari and coworkers analyzed reduced-representation bisulfite sequencing data for B-limphocytes, embryonic stem cells and testis cell lines, produced by ENCODE Project (ENCODE Project consortium, 2012). They observed an increased number of *de novo* mutations at sites which are known to be methylated, and this increase was particularly significant in the testis cell line. This demonstrates that DNA methylation and perhaps other cell type specific factors influence the occurrence of novel mutations. Since a high number of Cytosine to Tymine transitions in *SMAD4* exonic methylated CpG dinucleotides are reported to cause other germline and somatic disorders, it can be suggested that methylation may be an important regulatory mechanism of this gene, deregulation of which can result in the onset of several genetic conditions. Further studies are needed to better understand the role of methylation in regulating *SMAD4* mutation occurrence in different tissues and cell types.

6. Conclusions

Myhre syndrome (MYHRS, MIM 139210) is a rare sporadic autosomal developmental disorder for which around 50 cases are currently reported. Clinical features of MHYRS include typical facial gestalt (short palpebral fissures and philtrum, mid-face hypoplasia, prognathism, narrow mouth), thickened skin, joint limitation, muscular pseudohypertrophy, mild-to-moderate intellectual deficiency and hearing loss. This disorder is caused by missense mutations affecting the highly conserved MH2 domain of SMAD4 (Caputo *et al.*, 2012; Le Goff *et al.*, 2011a), the common mediator of TGFβ signaling pathway.

The main purpose of this thesis was the investigation of the molecular bases of Myhre syndrome. To reach this goal, functional and *in silico* approaches were carried out.

Western blot and immunofluorescence analysis demonstrated increased expression of SMAD4 Ile500 MYHRS mutants in respect to the wild type protein, disclosing an extra-nuclear accumulation under TGFβ stimulation. Moreover, we showed for the first time that Myhre mutations affecting the Ile500 residue have an anti-proliferative effect in primary fibroblasts and in mutant transfected cells. This finding suggests a loss of function effect for Myhre mutations on fibroblasts proliferation, which seems to abrogate the well-known proliferative role of TGFβ signaling in this cell type. Nevertheless, since the previously reported activation of TGFβ pathway in MYHRS cells (Piccolo *et al.*, 2014), further investigations directed to analyze the effect of SMAD4 protein accumulation on gene transcription and TGFβ signaling should be carried out, in order to clarify possible acquired functions of the mutated protein.

Furthermore, we collected and screened a cohort of 14 Myhre syndrome and Myhre-like cases, finding a *de novo* previously unreported c.1486 C>T transition at *SMAD4* codon 496 in 3 cases. Structural analysis of p.Arg496Cys amino acid change suggests that it could impair ubiquitination and, partially, the transcriptional activity of the complex itself as well. Even if structural data, as well as the overall homogeneous clinical phenotype of our p.Arg496Cys patients and p.Ile500 mutated cases, seem to confirm the functional equivalence between MYHRS Ile500 and Arg496, possible different effect of MYHRS mutations on TGFβ signaling and gene transcription should be investigated.

Since this transition arises in a CpG dinucleotide reported as methylated in several databases, we confirmed the methylation status of the involved cytosine by restriction enzyme assay.

These results suggest that methylation could be a regulatory mechanism acting on this gene, as suggested also by *in silico* analysis of CpG mutations in the entire *SMAD4* coding sequence.

Finally, cloning of genomic fragment and haplotypes analysis demonstrated exclusive paternal origin for Myhre causative mutations in all of 11 informative cases. This finding contributes to expand the number of point mutations causing dominant disorders which display a paternal bias in origin, and lead us to speculate on possibly other mechanisms which could produce a positive selection on MYHRS mutations in male testes.

7. Bibliography

Al Ageeli, E., Mignot, C., Afenjar, A., Whalen, S., Dorison, N., Mayer, M., Esteva, B., Dubern, B., Momtchilova, M., Le Gargasson, J.F., et al. (2012). Retinal involvement in two unrelated patients with Myhre syndrome. Eur. J. Med. Genet. *55*, 541-547.

Aran, D., Toperoff, G., Rosenberg, M., and Hellman, A. (2011). Replication timing-related and gene body-specific methylation of active human genes. Hum. Mol. Genet. *20*, 670–680.

Arnold, K., Bordoli, L., Kopp, J., and Schwede, T. (2006). The SWISS-MODEL Workspace: A web-based environment for protein structure homology modelling. Bioinformatics *22*, 195–201.

Asakura, Y., Muroya, K., Sato, T., Kurosawa, K., Nishimura, G., and Adachi, M. (2012). First case of a Japanese girl with Myhre syndrome due to a heterozygous *SMAD4* mutation. Am. J. Med. Genet. A *158A*, 1982-1986.

Attisano, L., and Lee-Hoeflick, S.T. (2001). The Smads. Genome Biol. *2*, S3010.1–S3010.8.

Bachmann-Gagescu, R., Hisama, F.M., and Yuen, A.L. (2011). Myhre syndrome with ataxia and cerebellar Atrophy. Clin. Dysmorphol. *20*, 156–159.

Becerra-Solano, L.E., Díaz-Rodriguez, M., Nastasi-Catanese, J.A., Toscano-Flores, J.J., Bañuelos-Robles, O., Figuera, L.E., Matute, E., and de Lourdes Ramírez-Dueñas, M. (2008). The fifth female patient with Myhre syndrome: Further delineation. Clin. Dysmorphol. *17*, 113–117.

Bottani, A., and Verloes, A. (1995). Myhre-GOMBO syndrome: Possible lumping of two ‘‘old’’ new syndromes. Am. J. Med. Genet. *59*, 523–524.

Bouras, M., Tabone, E., Bertholon, J., Sommer, P., Bouvier, R., Droz, J.P., and Benahmed, M. (2000). A novel *SMAD4* gene mutation in seminoma germ cell tumors. Cancer Res. *60*, 922-928.

Bourgeois, B., Gilquin, B., Tellier-Lebègue, C., Ostlund, C., Wu, W., Pèrez, J., El Hage, P., Lallemand, F., Worman, H.J., and Zinn-Justin, S. (2013). Inhibition of TGF-b signaling at the nuclear envelope: Characterization of interactions between MAN1, Smad2 and Smad3, and PPM1A. Sci. Signal. *6*, 280.

Buchberger, A., Howard, M.J., Proctor, M., and Bycroft, M. (2001). TheUBXdomain: A widespread ubiquitin-like module. J. Mol. Biol. *307*, 17–24.

Burglen, L., Héron, D., Moerman, A., Dieux-Coeslier, A., Bourguignon, J.P., Bachy, A., Carel, J.C., Cormier-Daire, V., Manouvrier, S., and Verloes, A. (2003). Myhre syndrome: New reports, review, and differential diagnosis. J. Med. Genet. *40*, 546–551.

Campbell, I.M., Stewart, J.R., James, R.A., Lupski, J.R., Stankiewicz, P., Olofsson, P., and Shaw, C.A. (2014). Parent of Origin, Mosaicism, and Recurrence Risk: Probabilistic Modeling Explains the Broken Symmetry of Transmission Genetics. Am. J. Hum. Genet. *95*, 345–359.

Caputo, V., Bocchinfuso, G., Castori, M., Traversa, A., Pizzuti, A., Stella, L., Grammatico, P., and Tartaglia, M. (2014). Novel SMAD4 mutation causing Myhre syndrome. Am. J. Med. Genet. A *164A*, 1835–1840.

Caputo, V., Cianetti, L., Niceta, M., Carta, C., Ciolfi, A., Bocchinfuso, G., Carrani, E., Dentici, M.L., Biamino, E., Belligni, E., et al. (2012). A Restricted Spectrum of Mutations in the *SMAD4* Tumor-Suppressor Gene Underlies Myhre Syndrome. Am. J. Hum. Genet. *90*, 161-169.

Carlson, K.M., Bracamontes, J., Jackson, C.E., Clark, R., Lacroix, A., Wells, S.A. Jr, and Goodfellow, P.J. (1994). Parent-of-origin effects in multiple endocrine neoplasia type 2B. Am. J. Hum. Genet. *55*, 1076-1082.

Chacko, B.M., Qin, B., Correia, J.J., Lam, S.S., de Caestecker, M.P., and Lin, K. (2001). The L3 loop and C-terminal phosphorylation jointly define Smad protein trimerization. Nat. Struct. Biol. *8*, 248–253.

Cook, W.J., Jeffrey, L.C., Carson, M., Chen, Z., and Pickart, C.M. (1992). Structure of a diubiquitin conjugate and a model for interaction with ubiquitin conjugating enzyme (E2). J. Biol. Chem. *267*, 16467–16471.

Coulondre, C., Miller, J.H., Farabaugh, P.J., and Gilbert, W. (1978). Molecular basis of base substitution hotspots in Escherichia coli. Nature *274*, 775-780.

Crow, J.F. (1997). The high spontaneous mutation rate: is it a health risk? Proc. Natl. Acad. Sci. *94*, 8380–8386.

Crow J.F. (2000). The origins, patterns and implications of human spontaneous mutation. Nat. Rev. Genet. *1*, 40-47.

Dagoneau, N., Benoist-Lasselin, C., Huber, C., Faivre, L., Mégarbané, A., Alswaid, A., Dollfus, H., Alembik, Y., Munnich, A., Legeai-Mallet, L., et al. (2004). ADAMTS10 mutations in autosomal recessive Weill-Marchesani syndrome. Am. J. Hum. Genet. *75*, 801-806.

Dávalos, N.O., García-Ortiz, J.E., García-Cruz, D., Feria-Velasco, A., and Sánchez-Corona, J. (2003). Clin. Dysmorphol. *12(2)*, 119-121.

de la Rochebrochard, E., McElreavey, K., and Thonneau, P. (2003). Paternal Age Over 40 Years: The "Amber Light" in the Reproductive Life of Men? J. Androl. *24*, 459–465.

Esterly, N.B., and McKusick, V.A. (1971). Stiff skin syndrome. Pediatrics. *47*,360-369.

Faivre, L., Dollfus, H., Lyonnet, S., Alembik, Y., Mégarbané, A., Samples, J., Gorlin, R.J., Alswaid, A., Feingold, J., Le Merrer, M., et al. (2003). Clinical homogeneity and genetic heterogeneity in Weill-Marchesani syndrome. Am. J. Med. Genet. A *123A*, 204-207.

Faivre, L., Gorlin, R.J., Wirtz, M.K., Godfrey, M., Dagoneau, N., Samples, J.R., Le Merrer, M., Collod-Beroud, G., Boileau, C., Munnich, A., and Cormier-Daire, V. (2003). In frame fibrillin-1 gene deletion in autosomal dominant Weill-Marchesani syndrome. J. Med. Genet. *40*, 34-36.

Faivre, L., Megarbane, A., Alswaid, A., Zylberberg, L., Aldohayan, N., Campos-Xavier, A.B., Bacq, D., Legeai-Mallet, L., Bonaventure, J., Munnich, A., and Cormier-Daire, V. (2002). Homozygosity mapping of a Weill-Marchesani syndrome locus to chromosome 19p13.3-p13.2. Hum. Genet. *110*, 366-370.

Fleming, N.I., Jorissen, R.N., Mouradov, D., Christie, M., Sakthianandeswaren, A., Palmieri, M., Day, F., Li, S., Tsui, C., Lipton, L., et al. (2013). SMAD2, SMAD3 and SMAD4 mutations in colorectal cancer. Cancer Res. *73*, 725–735.

Forbes, S.A., Beare, D., Gunasekaran, P., Leung, K., Bindal, N., Boutselakis, H., Ding, M., Bamford, S., Cole, C., Ward, S., et al. (2015). COSMIC: exploring the world's knowledge of somatic mutations in human cancer. Nucleic Acids Res. *43*, D805–D811.

Friedman, J.M. (1981). Genetic disease in the offspring of older fathers. Obstet. Gynecol. *57*, 745-749.

Gallione, C.J., Aylsworth, A.S., Beis, J., Berk, T., Bernhardt, B., Clark, R.D., Clericuzio, C., Danesino, C., Drautz, J., Fahl, J., et al. (2010). Overlapping spectra of *SMAD4* mutations in juvenile polyposis (JP) and JP-HHT syndrome. Am. J. Med. Genet. *152A*, 333–339.

Gallione, C.J., Repetto, G.M., Legius, E., Rustgi, A.K., Schelley, S.L., Tejpar, S. Mitchell, G., Drouin, E., Westermann, C.J., and Marchuk, D.A. (2004). A combined syndrome of juvenile polyposis and hereditary haemorrhagic telangiectasia associated with mutations in *MADH4* (*SMAD4*). Lancet *363*, 852–859.

Garcia-Cruz, D., Figuera, L.E., Feria-Velazco, A., Sánchez-Corona, J., Garcia-Cruz, M.O., Ramirez-Duenãs, R.M., Hernandez-Córdova, A., Ruiz, M.X., Bitar-Alatorre, W.E., Ramirez-Dueñas, M.L., et al. (1993). The Myhre syndrome: report of two cases. Clin. Genet. *44*, 203–207.

Gardner, H., Strehlow, D., Bradley, L., Widom, R., Farina, A., de Fougerolles, A., Peyman, J., Koteliansky, V., and Korn, J.H. (2004). Global expression analysis of the fibroblast transcriptional response to TGFbeta. Clin. Exp. Rheumatol. *22*, S47-S57.

Glaser, R.L., Jiang, W., Boyadjiev, S.A., Tran, A.K., Zachary, A.A., Van Maldergem, L., Johnson, D., Walsh, S., Oldridge, M., Wall, S.A., et al. (2000). Paternal origin of FGFR2 mutations in sporadic cases of Crouzon syndrome and Pfeiffer syndrome. Am. J. Hum. Genet. *66*, 768-777.

Glaser, R.L., Ramsay, J.P., and Morison, I.M. (2006). The imprinted gene and parent-of-origin effect database now includes parental origin of de novo mutations. Nucleic Acids Res. *34*, D29-D31.

Goriely, A., and Wilkie, A.O.M. (2012). Paternal Age Effect Mutations and Selfish Spermatogonial Selection: Causes and Consequences for Human Disease. Am. J. Hum. Genet. *90*, 175-200.

Gramley, F., Lorenzen, J., Koellensperger, E., Kettering, K., Weiss, C., and Munzel, T. (2010). Atrial fibrosis and atrial fibrillation: the role of the TGF-b1 signaling pathway. Int. J. Cardiol. *143*, 405–413.

Hackenberg, M., Barturen, G., and Oliver, J.L. (2011). NGSmethDB: a database for next-generation sequencing single-cytosine-resolution DNA methylation data. Nucleic Acids Res. *39*, D75-D79.

Hamosh, A., Scott, A.F., Amberger, J.S., Bocchini, C.A., and McKusick, V.A. (2005). Online Mendelian Inheritance in Man (OMIM), a knowledgebase of human genes and genetic disorders. Nucleic Acids Res. *33*, D514-D517.

Hawkes, L., and Kini, U. (2015). Myhre syndrome with facial paralysis and branch pulmonary stenosis. Clin. Dysmorphol. *24*, 84-85.

Huang, Y., Qi, Y., Du, J.Q., and Zhang, D.F. (2014). Micro RNA-34a regulates cardiac fibrosis after myocardial infarction by targeting Smad4. Expert Opin. Ther. Targets *12*, 1355–1365.

Ishibashi, N., Sasaki, Y., and Asakura, Y. (2014). Myhre syndrome: a rare craniofacial disorder. Cranio *32*, 300-306.

Jadayel, D., Fain, P., Upadhyaya, M., Ponder, M.A., Huson, S.M., Carey, J., Fryer, A., Mathew, C.G., Barker, D.F., and Ponder, B.A. (1990). Paternal origin of new mutations in von Recklinghausen neurofibromatosis. Nature *343*, 558-559.

Kato, M.V., Ishizaki, K., Shimizu, T., Ejima, Y., Tanooka, H., Takayama, J., Kaneko, A., Toguchida, J., and Sasaki, M.S. (1994). Parental origin of germ-line and somatic mutations in the retinoblastoma gene. Hum. Genet. *94*, 31-38.

Khalil, N., Xu, Y.D., O'Connor, R., and Duronio, V. (2005). Proliferation of pulmonary interstitial fibroblasts is mediated by transforming growth factor-beta1-induced release of extracellular fibroblast growth factor-2 and phosphorylation of p38 MAPK and JNK. J. Biol. Chem. *280*, 43000-43009.

Kong, A., Frigge, M.L., Masson, G., Besenbacher, S., Sulem, P., Magnusson, G., Gudjonsson, S.A., Sigurdsson, A., Jonasdottir, A., Jonasdottir, A., et al. (2012). Rate of de novo mutations and the importance of father's age to disease risk. Nature *488*, 471-475.

Kuang, C., and Chen, Y. (2004). Tumor-derived C-terminal mutations of Smad4 with decreased DNA binding activity and enhanced intramolecular interaction. Oncogene *23*, 1021–1029.

Kutz, W.E., Wang, L.W., Bader, H.L., Majors, A.K., Iwata, K., Traboulsi, E.I, Sakai, L.Y., Keene, D.R., and Apte, S.S. (2011). ADAMTS10 protein interacts with fibrillin-1 and promotes its deposition in extracellular matrix of cultured fibroblasts. J. Biol. Chem. *286*, 17156-17167.

Landrum, M.J., Lee, J.M., Riley, G.R., Jang, W., Rubinstein, W.S., Church, D.M., and Maglott, D.R. (2014). ClinVar: public archive of relationships among sequence variation and human phenotype. Nucleic Acids Res. *42*, D980-D985.

Lazzereschi, D., Nardi, F., Turco, A., Ottini, L., D'Amico, C., Mariani-Costantini, R., Gulino, A., and Coppa, A. (2005). A complex pattern of mutations and abnormal splicing of Smad4 is present in thyroid tumours. Oncogene *24*, 5344–5354.

Le Goff, C., and Cormier-Daire, V. (2012). From tall to short: the role of TGFβ signaling in growth and its disorders. Am. J. Med. Genet. C *160C*, 145-153.

Le Goff, C., Mahaut, C., Abhyankar, A., Le Goff, W., Serre, V., Afenjar, A., Destrée, A., di Rocco, M., Héron, D., Jacquemont, S., et al. (2011). Mutations at a single codon in Mad homology 2 domain of SMAD4 cause Myhre syndrome. Nat. Genet. *44*, 85–88.

Le Goff, C., Mahaut, C., Wang, L. W., Allali, S., Abhyankar, A., Jensen, S., Zylberberg, L., Collod-Beroud, G., Bonnet, D., Alanay, Y., et al. (2011). Mutations in the TGF-beta binding-protein-like domain 5 of FBN1 are responsible for acromicric and geleophysic dysplasias. Am. J. Hum. Genet. *89*, 7-14.

Le Goff, C., Morice-Picard, F., Dagoneau, N., Wang, L.W., Perrot, C., Crow, Y.J., Bauer, F., Flori, E., Prost-Squarcioni, C., Krakow, D., et al. (2008). ADAMTSL2 mutations in geleophysic dysplasia demonstrate a role for ADAMTS-like proteins in TGF-beta bioavailability regulation. Nat. Genet. *40*, 1119-1123.

Lindor, N.M. (2009). LAPS syndrome and Myhre syndrome: two disorders or one? Am. J. Med. Genet. A *149A*, 798-799.

Lindor, N.M., Gunawardena, S.R., and Thibodeau, S.N. (2012). Mutations of *SMAD4* account for both LAPS and Myhre syndromes. Am. J. Med. Genet. A *158A*, 1520-1521.

Lindor, N.M., Kasperbauer, J.L., Hoffman, A.D., Parisi, J.E., Wang, H., and Warman, M. (2002). Confirmation of existence of a new syndrome: LAPS syndrome. Am. J. Med. Genet. *109(2)*, 93-99.

Lister, R., Pelizzola, M., Dowen, R.H., Hawkins, R.D., Hon, G., Tonti-Filippini, J., Nery, J.R., Lee, L., Ye, Z., Ngo, Q.M., et al. (2009). Human DNA methylomes at base resolution show widespread epigenomic differences. Nature *462*, 315–322.

Loeys, B.L., Gerber, E.E., Riegert-Johnson, D., Iqbal, S., Whiteman, P., McConnell, V., Chillakuri, C.R., Macaya, D., Coucke, P.J., De Paepe, A., et al. (2010). Mutations in fibrillin-1 cause congenital scleroderma: stiff skin syndrome. Sci. Transl. Med. *23*, 23ra20.

Lopez-Cardona, M.G., Garcia-Cruz, D., Garcia-Ortiz, J.E., Davalos, N.O., Feria-Velasco, A., Rodriguez-Rojas, L.X., Garcia-Cruz, M.O., Figuera-Villanueva, L.E., Stephens, A., Larios-Arceo, F., and Sanchez-Corona, J. (2004). Second female case of Myhre syndrome. Clin. Dysmorphol. *13*, 91–94.

Magis, C., Gasparini, D., Lecoq, A., Le Du, M.H., Stura, E., Charbonnier, J.B, Mourier, G., Boulain, J.C., Pardo, L., Caruana, A., et al. (2006). Structure-based secondary structure-independent

approach to design protein ligands: Application to the design of Kv1.2 potassium channel blockers. J. Am. Chem. Soc. *128*, 16190–161205.

Maher, G.J., Goriely, A., and Wilkie, A.O. (2014). Cellular evidence for selfish spermatogonial selection in aged human testes. Andrology *2*, 304-314.

Marchesani, O. (1939). Brachydaktylie und angeborene Kugellinse als Systemerkrankung. Klin. Monatsbl. Augenheilkd. *103*, 392-406.

Maroteaux, P., Stanescu, R., Stanescu, V., and Rappaport, R. (1986). Acromicric dysplasia. Am. J. Med. Genet. *24*, 447-459.

Martinelli, S., Torreri, P., Tinti, M., Stella, L., Bocchinfuso, G., Flex, E., Grottesi, A., Ceccarini, M., Palleschi, A., Cesareni, G., et al. (2008). Diverse driving forces underlie the invariant occurrence of the T42A, E139D, I282V and T468M SHP2 amino acid substitutions causing Noonan and LEOPARD syndromes. Hum. Mol. Genet. *17*, 2018-2029.

Massagué , J. (1998). TGF-beta signal transduction. Annu. Rev. Biochem. *67*, 753–791.

Massagué, J., Blain, S.W., and Lo, R.S. (2000). TGFbeta signaling in growth control, cancer, and heritable disorders. Cell *103*, 295–309.

Massagué, J., and Gomis, R.R. (2006). The logic of TGFbeta signaling. FEBS Lett. *580*, 2811-2820.

Massagué, J., Seoane, J., and Wotton, D. (2005). Smad transcription factors. Genes Dev. *19*, 2783–2810.

Maunakea, A.K., Nagarajan, R.P., Bilenky, M., Ballinger, T.J., D'Souza, C., Fouse, S.D., Johnson, B.E., Hong, C., Nielsen, C., Zhao, Y., et al. (2010). Conserved role of intragenic DNA methylation in regulating alternative promoters. Nature *466*, 253–257.

McGowan, R., Gulati, R., McHenry, P., Cooke, A., Butler, S., Keng, W.T., Murday, V., Whiteford, M., Dikkers, F.G., Sikkema-Raddatz, B., et al. (2011). Clinical features and respiratory complications in Myhre syndrome. Eur. J. Med. Genet. *54*, 553-559.

Meyer, S. J., and Holstein, T. (1941). Spherophakia with glaucoma and brachydactyly. Am. J. Ophthal. *24*, 247-257.

Michot, C., Le Goff, C., Mahaut, C., Afenjar, A., Brooks, A.S., Campeau, P.M., Destree, A., Di Rocco, M., Donnai, D., Hennekam, R., et al. (2014). Myhre and LAPS syndromes: clinical and molecular review of 32 patients. Eur. J. Hum. Genet. *22*, 1272-1277.

Moloney, D.M., Slaney, S.F., Oldridge, M., Wall,, S.A., Sahlin, P., Stenman, G., and Wilkie, A.O. (1996). Exclusive paternal origin of new mutations in Apert syndrome. Nat. Genet. *13*, 48-53.

Moore, W.T., and Federman, D.D. (1965). Familial dwarfism and "stiff joints". Arch. Intern. Med. *115*, 398-404.

Myhre, S.A., Ruvalcaba, R.H.A., and Graham, C.B. (1981). A new growth deficiency syndrome. Clin. Genet. *20*, 1–5.

Pettersen, E.F., Goddard, T.D., Huang, C.C., Couch, G.S., Greenblatt, D.M., Meng, E.C., and Ferrin, T.E. (2004). UCSF Chimera- a visualization system for exploratory research and analysis. J. Comput. Chem. *25*, 1605–1612.

Picco, P., Naselli, A., Pala, G., Marsciani, A., Buoncompagni, A., and Martini, A. (2013). Recurrent pericarditis in Myhre syndrome. Am. J. Med. Genet. A *161A*, 1164-1166.

Piccolo, P., Mithbaokar, P., Sabatino, V., Tolmie, J., Melis, D., Schiaffino, M.C., Filocamo, M., Andria, G., and Brunetti-Pierri, N. (2014). *SMAD4* mutations causing Myhre syndrome result in disorganization of extracellular matrix improved by losartan. Eur. J. Hum. Genet. *22*, 988-994.

Rahbari, R., Wuster, A., Lindsay, S.J., Hardwick, R.J., Alexandrov, L.B., Al Turki, S., Dominiczak, A., Morris, A., Porteous, D., Smith, B., et al. (2016). Timing, rates and spectra of human germline mutation. Nat. Genet. *48*, 126-133.

Rannan-Eliya, S.V., Taylor, I.B., de Heer, I.M., van den Ouweland, A.M., Wall, S.A., and Wilkie, A.O. (2004). Paternal origin of FGFR3 mutations in Muenke-type craniosynostosis. Hum. Genet. *115*, 200-207.

Rulli, I., Ferrero, G.B., Belligni, E., Delmonaco, A.G., Defilippi, C., and Silengo, M. (2005). Myhre's syndrome in a girl with normal intelligence. Am. J. Med. Genet. A. *134A*, 100–102.

Schuffenecker, I., Ginet, N., Goldgar, D., Eng, C., Chambe, B., Boneu, A., Houdent, C., Pallo, D., Schlumberger, M., Thivolet, C., et al. (1997). Prevalence and parental origin of de novo RET mutations in multiple endocrine neoplasia type 2A and familial medullary thyroid carcinoma. Le Groupe d'Etude des Tumeurs a Calcitonine. Am. J. Hum. Genet. *60*, 233-237.

Sherry, S.T., Ward, M.H., Kholodov, M., Baker, J., Phan, L., Smigielski, E.M., and Sirotkin, K. (2001). dbSNP: the NCBI database of genetic variation. Nucleic Acids Res. *29*, 308-311.

Singer, M., Kosti, I., Pachter, L., and Mandel-Gutfreund, Y. (2015). A diverse epigenetic landscape at human exons with implication for expression. Nucleic Acids Res. *43*, 3498-508.

Snajderova, M., Riccardi, V.M., Petrak, B., Zemkova, D., Zapletalova, J., Mardesic, T., Petrakova, A., Lanska, V., Marikova, T., Bendova, S., et al. (2012). The importance of advanced parental age in the origin of neurofibromatosis type 1. Am. J. Med. Genet. A. *158A*, 519-523.

Sol-Church, K., Stabley, D.L., Nicholson, L., Gonzalez, I.L., and Gripp, K.W. (2006). Paternal bias in parental origin of HRAS mutations in Costello syndrome. Hum. Mutat. *27*, 736-741.

Soljak, M.A., Aftimos, S., and Gluckman, P.D. (1983), A new syndrome of short stature, joint limitation and muscle hypertrophy. Clin. Genet. *23,* 441–446.

Spranger, J.W., Gilbert, E.F., Tuffli, G.A., Rossiter, F.P., and Opitz, J.M. (1971). Geleophysic dwarfism--a "focal" mucopolysaccharidosis? Lancet *298*, 97-98.

Starr, L.J., Grange, D.K., Delaney, J.W., Yetman, A.T., Hammel, J.M., Sanmann, J.N., Perry, D.A., Schaefer, G.B., and Olney, A.H. (2015). Myhre syndrome: Clinical features and restrictive cardiopulmonary complications. Am. J. Med. Genet. A *167*, 2893-2901.

Tartaglia, M., Cordeddu, V., Chang, H., Shaw, A., Kalidas, K., Crosby, A., Patton, M.A., Sorcini, M., van der Burgt, I., Jeffery, S., et al. (2004). Paternal germline origin and sex-ratio distortion in transmission of PTPN11 mutations in Noonan syndrome. Am. J. Hum. Genet. *75*, 492-497.

Thomas, G.H. (1996). High male:female ratio of germ-line mutations: An alternative explanation for postulated gestational lethality in males in X-linked dominant disorders. Am. J. Hum. Genet. *58*, 1364–1368.

Titomanlio, L., Marzano, M.G., Rossi, E., D'Armiento, M., De Brasi, D., Vega, G.R., Andreucci, M.V., Orsini, A.V., Santoro, L., and Sebastio, G. (2001). Case of Myhre syndrome with autism and peculiar skin histological findings. Am. J. Med. Genet. *103*, 163–165.

Toriello, H.V., and Meck, J.M. (2008). Statement on guidance for genetic counseling in advanced paternal age. Genet. Med. *10*, 457-460.

Trappe, R., Laccone, F., Cobilanschi, J., Meins, M., Huppke, P., Hanefeld, F., and Engel, W. (2001). MECP2 mutations in sporadic cases of Rett syndrome are almost exclusively of paternal origin. Am. J. Hum. Genet. *68*, 1093-1101.

van Steensel, M.A.M., Vreeburg, M., Steijlen, P.M., and de Die-Smulders, C. (2005). Myhre syndrome in a female with previously undescribed symptoms: Further delineation of the phenotype. Am. J. Med. Genet. A *139A*, 127–130.

Varley, K.E., Gertz, J., Bowling, K.M., Parker, S.L., Reddy, T.E., Pauli-Behn, F., Cross, M.K., Williams, B.A., Stamatoyannopoulos, J.A., Crawford, G.E., et al. (2013). Dynamic DNA methylation across diverse human cell lines and tissues. Genome Res. *23*, 555–567.

Verloes, A., Delfortrie, J., and Lambotte, C. (1989). GOMBO syndrome of growth retardation, ocular abnormalities, microcephaly, brachydactyly, and oligophrenia: a possible "new" recessively inherited MCA/MR syndrome. Am. J. Med. Genet. *32*, 15-18.

Verloes, A., Lesenfants, S., Jamar, M., Dideberg, V., and Herens, C. (2000). GOMBO syndrome: another “pseudorecessive” disorder due to a cryptic translocation. Am. J. Med. Genet. *95*, 185–186.

Wang, J., Xu, N., Feng, X., Hou, N., Zhang, J., Cheng, X., Chen, Y., Zhang, Y., and Yang, X. (2005). Targeted disruption of Smad4 in cardiomyocytes results in cardiac hypertrophy and heart failure. Circ. Res. *14*, 821–828.

Weill, G. (1932). Ectopie du cristillins et malformations generales. Ann. Oculist. *169*, 21-44.

Whiteford, M.L., Doig, W.B., Raine, P.A.M., Hollman, A.S., and Tolmie, J.L. (2001). A new case of Myhre syndrome. Clin. Dysmorphol. *10*, 135-140.

Wilkin, D.J., Szabo, J.K., Cameron, R., Henderson, S., Bellus, G.A., Mack, M.L., Kaitila, I., Loughlin, J., Munnich, A., Sykes, B., et al. (1998). Mutations in fibroblast growth-factor receptor 3 in sporadic cases of achondroplasia occur exclusively on the paternally derived chromosome. Am. J. Hum. Genet. *63*, 711-716.

Winter, R.M., Patton, M.A., Challener, J., Mueller, R.F., and Baraitser, M. (1989). Moore-Federman syndrome and acromicric dysplasia: are they the same entity? J. Med. Genet. *26*, 320-325.

Wong, W.S., Solomon, B.D., Bodian, D.L., Kothiyal, P., Eley, G., Huddleston, K.C., Baker, R., Thach, D.C., Iyer, R.K., Vockley, J.G., and Niederhuber, J.E. (2016). New observations on maternal age effect on germline de novo mutations. Nat. Commun. *7*, 10486.

Wu, J.W., Hu, M., Chai, J., Seoane, J., Huse, M., Li, C., Rigotti, D.J., Kyin, S., Muir, T.W., Fairman, R., et al. (2001). Crystal structure of a phosphorylated Smad2: Recognition of phosphoserine by the MH2 domain and insights on Smad function in TGF-beta signaling. Mol. Cell. *8*, 1277–1289.

8. Publications and poster/oral communications presented at scientific congress

Caputo, V., Bocchinfuso, G., Castori, M., Traversa, A., Pizzuti, A., Stella, L., Grammatico, P., and Tartaglia, M. (2014). Novel *SMAD4* mutation causing Myhre syndrome. Am. J. Med. Genet. A. *164*(7), 1835-40.

Niceta, M., Stellacci, E., Gripp, K. W., Zampino, G., Kousi, M., Anselmi, M., Traversa, A., Ciolfi, A., Stabley, D., Bruselles, A., et al. (2015). Mutations Impairing GSK3-Mediated MAF Phosphorylation Cause Cataract, Deafness, Intellectual Disability, Seizures, and a Down Syndrome-like Facies. Am. J. Hum. Genet. *96(5)*, 816-825.

Niceta, M., Stellacci, E., Gripp, K. W., Zampino, G., Traversa, A., Ciolfi, A., Bruselles, A., Caputo, V., Keppler-Noreuil, K., Niyazov, D. M., et al. (2014). Missense mutations in *MAF* cause Fine-Lubinsky Syndrome. SIGU 2014 - oral comunication.

Niceta, M., Stellacci, E., Gripp, K. W., Zampino, G., Traversa, A., Ciolfi, A., Bruselles, A., Caputo, V., Keppler-Noreuil, K., Niyazov, et al. (2014). Missense mutations in *MAF* cause Fine-Lubinsky Syndrome. ESHG 2014 - oral comunication.

Traversa, A., Caputo, V., Bocchinfuso, G., Stella, L., Pizzuti, A. and Tartaglia, M. (2015). Novel mutation in the *SMAD4* Tumor-Suppressor gene causing Myhre syndrome: molecular and structural studies. BeMM symposium 2015 - poster.

Traversa, A., Cordeddu, V., Bocchinfuso, G., Stella, L., Silengo, M., Ferrero, G. B., Castori, M., Grammatico, P., Boccone, L., Garavelli, L., et al. (2015). Molecular characterization of Myhre Syndrome. SIGU 2015 - poster.

Niceta, M., Stellacci, E., Traversa, A., Gripp, K. W., Zampino, G., Ciolfi, A., Bruselles, A., Caputo, V., Keppler-Noreuil, K., Niyazov, D. M., et al. (2016). Missense mutations in *MAF* cause Fine-Lubinsky Syndrome. 6th BeMM symposium - oral comunication.